Novel epigenetic-metabolic inhibitor combination treatment blocks platinum-induced ovarian cancer stem cell enrichment

Riddhi Sood[1], Sikai Xiao[2], Shruthi Sriramkumar[2], Christiane Hassel[3], Kenneth P. Nephew[2,4,5], Heather M. O'Hagan[2,4,6,#]

[1]Genome, Cell and Developmental Biology, Department of Biology, Indiana University Bloomington, Bloomington, IN, 47405, USA

[2]Cell, Molecular and Cancer Biology Graduate Program and Medical Sciences Program, Indiana University School of Medicine, Bloomington, IN, 47405, USA

[3]Flow Cytometry Core Facility, Department of Biology, Indiana University, Bloomington, IN 47405, USA

[4]Indiana University Melvin and Bren Simon Comprehensive Cancer Center, Indianapolis, IN, 46202, USA

[5]Department of Anatomy, Cell Biology and Physiology; Department of Obstetrics and Gynecology, Indiana University School of Medicine, Indianapolis, IN, 46202, USA

[6]Department of Medical and Molecular Genetics, Indiana University School of Medicine, Indianapolis, IN, 46202, USA

[#]Corresponding author. 1001 East 3rd Street, Bloomington, IN 47405. (812) 855-3035. hmohagan@indiana.edu.

Conflict of interest: The authors declare no conflict of interest.

Key words: BRCA1, DNA hypermethylation, chemoresistance, ovarian cancer, DNA damage response, NAD^+, ovarian cancer stem cells, DNMT inhibitor, NAMPT

Abstract

High grade serous ovarian cancer (HGSOC) is the most common and aggressive type of ovarian cancer. Platinum resistance is a common occurrence in HGSOC and a main cause of tumor relapse resulting in high patient mortality rates. Recurrent ovarian cancer is enriched in aldehyde dehydrogenase (ALDH)+ ovarian cancer stem cells (OCSCs), which are resistant to platinum agents. We demonstrated that acute platinum treatment induced a DNA damage-dependent decrease in BRCA1 levels through *BRCA1* promoter DNA hypermethylation. In a parallel pathway associated with G2/M arrest, platinum treatment also induced an increase in expression of *NAMPT*, the rate limiting regulator of NAD^+ production from the salvage pathway, and NAD^+ levels, the cofactor required for ALDH activity. Both decreased BRCA1 and increased NAD^+ levels were required for the platinum-induced enrichment of OCSCs, and inhibition of both DNA methyltransferases (DNMT) and NAMPT synergistically abrogated the platinum-induced increase in OCSCs. We conclude that these two separate pathways lead to platinum-induced OCSC enrichment, providing preclinical evidence that in the neoadjuvant setting, combining DNMT and NAMPT inhibitors with platinum has the potential to reduce OC reoccurrence.

Introduction

Ovarian cancer (OC) is the 5th leading cause of cancer related death among women (1). High grade serous ovarian cancer (HGSOC), the most aggressive type of OC, accounts for 70-80% of all OC cases (1). The majority of OC cases are detected at an advanced stage and survival rate for patients diagnosed with stage IV disease is a dismal 17% (2). The primary therapy for the management of advanced stage OC continues to include a combination of surgery and chemotherapy and while most patients achieve a complete remission, the majority will recur and subsequently develop chemotherapy resistant disease (3).

We and others have shown that a subpopulation of cells called ovarian cancer stem cells (OCSCs) preferentially survive after treatment with platinum-based chemotherapeutic drugs (4), are enriched in recurrent tumors (5) and are at least partially responsible for chemotherapy resistance (6). Several markers have been used to identify OCSCs, including the activity of aldehyde dehydrogenase (ALDH) enzymes. ALDH1 is overexpressed in OCSCs and *ALDH1* expression correlates with worse OC survival and platinum resistance (4, 7). ALDH+ cells have tumor initiating capacity, form spheroids in non-adherent conditions, and express stem cell markers (4, 8), all criteria of functional CSCs.

Standard of care platinum-based chemotherapeutic drugs (cisplatin, carboplatin) cause DNA damage in the form of platinum-DNA adducts (9), which activate the DNA damage response (DDR). The DDR can result in DNA repair, cell cycle arrest, and/or apoptosis (10, 11). Altered DDR is thought to contribute to the ability of OCSCs to survive chemotherapy. For example, OCSCs have higher levels of DDR pathway activation through phosphorylation of DDR factors like ataxia telangiectasia mutated (ATM), checkpoint kinase 1 (CHK1) and CHK2 (12). The tumor suppressor

breast cancer 1 (BRCA1) plays an important role in regulating the DDR through interaction of its various functional domains with proteins required for cell cycle regulation, tumor suppression, and DNA repair (13-16). About 40% of women with a family history of OC have *BRCA1/2* mutation or promoter hypermethylation (2).

Tumors with *BRCA1* mutation frequently undergo locus-specific loss of heterozygosity (LOH), resulting in loss of the wildtype copy of *BRCA1* and subsequent increased sensitivity to chemotherapy due to defective homologous recombination DNA repair (17). Patients with *BRCA1* mutant tumors without locus-specific LOH have significantly lower percentage of survival compared to patients with *BRCA1* mutation with locus-specific LOH (17), indicating partial loss of BRCA1 functions as a secondary mode of resistance to chemotherapy. Furthermore, as survival rates of patients with BRCA1 promoter DNA hypermethylation were lower compared to patients with BRCA1 mutation (18), and the fact the vast majority of HGSOC have a wildtype *BRCA1* (2), a better understanding of the role of wildtype BRCA1 in response to platinum agents is of critical importance.

The metabolite nicotinamide adenine dinucleotide (NAD^+) plays a key role in major metabolic pathways including glycolysis, tricarboxylic acid (TCA) cycle, and oxidative phosphorylation (19). Furthermore, NAD^+ is a co-factor for ALDH enzymes and essential for the ALDH-mediated conversion of aldehydes to carboxylic acids (20, 21). Ovarian tumors with reduced expression of *BRCA1* through *BRCA1* promoter DNA hypermethylation or mutation have increased levels of NAD^+ and expression of nicotinamide phosphoribosyltranferase (NAMPT), the rate limiting regulator of NAD^+ synthesis from the salvage pathway (22). Furthermore, NAMPT has been shown to promote platinum-induced senescence-associated OCSCs (23). Therefore,

84 studying the role of metabolites in the response to platinum treatment is important to
85 understand how chemoresistance develops.

86 With OCSCs known involvement in chemoresistance and tumor reoccurrence, we sought
87 to mechanistically study how platinum treatment induces OCSC enrichment and develop
88 strategies to combat this enrichment. We demonstrate that two separate pathways drive
89 platinum-induced OCSC enrichment, one involving epigenetic-mediated silencing of BRCA1 and
90 the other altered energy metabolism. Cisplatin treatment resulted in a DDR-dependent decrease
91 in *BRCA1* expression through *BRCA1* promoter DNA hypermethylation as well as a G2/M cell cycle
92 arrest-related increase in *NAMPT* expression and subsequent increase in cellular NAD^+ levels.
93 Importantly, combined treatment with a DNA methyltranferase (DNMT) and a NAMPT inhibitor
94 synergistically abrogated the cisplatin-induced OCSC enrichment. Our findings support using a
95 novel epigenetic-metabolic inhibitor combination in the neoadjuvant setting to reduce the
96 platinum-induced enrichment of OCSCs and avert the development of platinum resistance in OC.
97

98 **Results**

99 **Cisplatin treatment enriches for ALDH+ cells**

100 Advanced stage OC patients frequently have residual tumor cells following
101 chemotherapy. To determine whether OCSCs are enriched by platinum chemotherapy, we
102 treated HGSOC cell lines OVCAR5, OVSAHO and OVCAR3 with corresponding IC_{50} doses of
103 cisplatin (24) and analyzed the percentage of ALDH+ (%ALDH+) cells using the ALDEFLUOR assay
104 (4). To investigate acute effects, we first conducted a time course study in OVCAR5 cells (3 to 16
105 h). The %ALDH+ cells significantly increased after treatment with cisplatin for 8 h and 16 h (Fig.

1A, Supplementary Fig. S1A). Similarly, cisplatin treatment for 16 h increased the %ALDH+ cells in OVSAHO (5.8% to 10.8%) and OVCAR3 (20% to 28%) cell lines (Fig. 1A). PEO1, a *BRCA2* mutant OC cell line (25), had lower initial levels of %ALDH+ cells and a smaller but significant cisplatin-induced increase in %ALDH+ cells at 16 h (Supplementary Fig. S1B). However, in the *BRCA1* mutant COV362 (26) cell line, no increase in %ALDH+ cells after acute cisplatin treatment was observed (Supplementary Fig. S1B). To confirm that the increase in %ALDH+ cells was associated with a stemness phenotype, we tested the ability of platinum-treated OVCAR5 and OVSAHO cells to form spheroids in anchorage independent conditions. When cells were plated in stem cell media, cisplatin pretreated cells were more spheroid-like compared to UT (Fig. 1B). Using a cell viability assay based on intracellular esterase activity, there were significantly more viable cells in the spheroids generated from cells pretreated with cisplatin than from UT cells (Fig. 1B).

Isotypes of ALDH1 - *ALDH1A1*, *ALDH1A2* and *ALDH1A3* are linked to stemness of OC cells (27). Depending on the tumor type and cell line, different isozymes of ALDH1 are overexpressed – *ALDH1A3* in OVCAR5 and *ALDH1A1* in OVSAHO (Supplementary Fig. S1C). We hypothesized that cisplatin may induce enrichment of ALDH+ cells by altering ALDH expression. However, no change in expression of *ALDH1A1/A2/A3* isoforms after treatment with cisplatin was observed in OVCAR5 cells (Supplementary Fig. S1C). In OVSAHO cells, no change in expression of the major ALDH1 isoform in these cells, *ALDH1A1*, was observed after cisplatin treatment, although *ALDH1A2* and *ALDH1A3* isoforms significantly decreased and increased, respectively, after cisplatin treatment (Supplementary Fig. S1C). Because *ALDH1A1* is expressed approximately 100-fold more than *ALDH1A3*, *ALDH1A1* likely contributes to the majority of ALDH activity in this cell line suggesting the change in *ALDH1A3* expression has no detectable effect on ALDH activity.

Additionally, even though cisplatin caused the expected increase in the DNA damage marker phosphorylated histone 2AX (γH2AX) over a cisplatin time course, there was no significant change in ALDH1 protein levels in OVCAR5 cells (Supplementary Fig. 1D).

BRCA1 is known to play a role in OC (2) and the DDR (13-16). As BRCA1 levels have been linked to an interstrand crosslink (ICL)-dependent increase in stemness (28), we assayed BRCA1 expression following cisplatin treatment. *BRCA1* RNA expression levels in OVCAR5, OVSAHO and *BRCA2*-mutant PEO1 significantly decreased by 16 h after cisplatin treatment (Fig. 1C). Furthermore, BRCA1 protein levels correspondingly decreased and correlated with increased γH2AX levels in cisplatin treated cells (Fig. 1D). Taken together, these data suggest that acute cisplatin treatment enriched for ALDH+ cells with stemness properties and decreased *BRCA1* levels. The minimal change in ALDH1 level after cisplatin treatment further suggested that another mechanism contributes to the cisplatin-induced enrichment of ALDH+ cells.

The cisplatin-induced decrease in *BRCA1* levels is associated with *BRCA1* promoter DNA hypermethylation

BRCA1 expression is regulated through different mechanisms, including promoter DNA hypermethylation-associated gene silencing (29). Corresponding to the platinum-induced decrease in BRCA1 expression, there was a significant increase in *BRCA1* promoter DNA methylation after 3 h, 8 h and 16 h cisplatin treatment as assayed by quantitative methylation-specific PCR (qMSP) in OVCAR5 and OVSAHO cells (Fig. 2A). Bisulfite sequencing of 12 CpG sites within the *BRCA1* promoter region confirmed the increase in methylated CpGs after 16 h cisplatin treatment compared to untreated (UT) cells (Fig. 2B). Total methylation percentage calculated

using the bisulfite sequencing data further demonstrated an increase in *BRCA1* promoter DNA methylation after cisplatin treatment (Fig. 2C).

DNA methylation is catalyzed by DNMTs. DNMT1 is predominantly a maintenance DNA methyltransferase whereas DNMT3B and DNMT3A are predominantly *de novo* DNMTs (30). Cisplatin treatment increased the levels of DNMT1 and DNMT3B protein (Fig. 2D), corresponding to the timing of the *BRCA1* promoter hypermethylation and increase in the DNA damage marker γH2AX (Fig. 2D). Altogether this data demonstrates that the cisplatin-induced decrease in *BRCA1* expression is associated with promoter DNA hypermethylation.

The cisplatin-induced decrease in BRCA1 is essential for the associated increase in %ALDH+ cells

To determine if a decrease in *BRCA1* expression is sufficient to increase the %ALDH+ cells, we altered BRCA1 levels by using stable shRNA mediated knockdown (KD) in OVCAR5 cells. BRCA1 KD using two different shRNAs reduced *BRCA1* expression compared to empty vector (EV) shRNA cells to level similar to EV cells treated with cisplatin (Fig. 3A). Additionally, BRCA1 protein levels decreased after BRCA1 KD compared to EV to a level similar to EV cells treated with cisplatin (Fig. 3B). BRCA1 shRNA1 KD cells had similar baseline %ALDH+ cells compared to EV (Fig. 3C). The slight increase in %ALDH+ cells in BRCA1 shRNA2 KD compared to EV cells was significantly less than the cisplatin-induced increase in EV cells.

Because the effect of altering BRCA1 levels on the %ALDH+ cells was limited, we hypothesized that DNA damage caused by cisplatin is important to induce an increase in %ALDH+ cells. ATM, one of the first proteins to be recruited to DNA damage sites (31), is responsible for phosphorylation of downstream targets like H2AX and the activation of downstream DNA repair

pathways (32). Inhibiting ATM (ATMi) using KU-55933 (30) reduced cisplatin-induced levels of active, phosphorylated ATM in OVCAR5 and OVSAHO cells (Supplementary Fig. S2A). Consistent with our previous results (Fig. 1C), *BRCA1* levels decreased after cisplatin only treatment (Fig. 3D). *BRCA1* expression after treatment with ATMi only was similar to DMSO treated in both cell lines (Fig. 3D). ATMi and cisplatin dual treatment prevented the cisplatin-induced decrease in *BRCA1* expression, with *BRCA1* levels being similar to DMSO treated cells in both cell lines. Consistent with the association between decreased *BRCA1* levels and increased %ALDH+ cells, combining ATMi with cisplatin treatment prevented the cisplatin-induced increase in %ALDH+ cells compared to cisplatin treatment only in both cell lines (Fig. 3E). ATMi treatment itself did not alter the %ALDH+ cells in OVCAR5 cells but decreased the %ALDH+ cells compared to DMSO treated cells in OVSAHO cells (Fig. 3E).

Next, we transiently transfected cells with a plasmid that drives expression of *BRCA1* using an exogenous promoter lacking the normal *BRCA1* regulatory regions, including the promoter CpG island (CpGi-null BRCA1; Supplementary Fig. 2B). Cells transfected with CpGi-null BRCA1 had higher levels of *BRCA1* expression when compared to UT EV transfected cells in OVCAR5 and OVSAHO cells (Fig. 3F). Cisplatin treatment decreased *BRCA1* expression in CpGi-null BRCA1 transfected OVSAHO cells but not in OVCAR5 cells compared to UT CpGi-null BRCA1 transfected cells but *BRCA1* levels remained higher than EV cells treated with or without cisplatin in both cell lines (Fig. 3F). Similarly, BRCA1 protein levels were higher in UT CpGi-null BRCA1 transfected OVCAR5 cells compared to UT EV transfected cells (Fig. 3G). BRCA1 protein levels decreased in cisplatin-treated CpGi-null BRCA1 transfected cells compared to UT CpGi-null BRCA1 and UT EV transfected cells but remained higher than cisplatin treated EV transfected cells (Fig. 3G). As

194 expected, γH2AX levels increased in cells treated with cisplatin with EV or CpGi-null BRCA1
195 transfection (Fig. 3G).

196 To determine how maintaining BRCA1 levels effects platinum-induced OCSC enrichment,
197 the ALDFLUOR assay was performed in UT and cisplatin-treated EV and CpGi-null BRCA1
198 transfected cells. UT CpGi-null BRCA1 transfected cells had similar baseline %ALDH+ cells as UT
199 EV transfected cells in both OVCAR5 and OVSAHO cells (Fig. 3H). Importantly, even though
200 cisplatin increased the %ALDH+ cells in EV cells as expected, there was no increase in %ALDH+
201 cells after cisplatin treatment in CpGi-null BRCA1 transfected cells in both cell lines. Collectively,
202 these data demonstrate that the effect of altering BRCA1 levels without DNA damage on %ALDH+
203 cells is limited, maintaining BRCA1 expression prevents the platinum-induced increase in %ALDH+
204 cells and the cisplatin-induced decrease in BRCA1 levels below the level in EV cells contributes to
205 the cisplatin-induced increase in %ALDH+ cells.

206

207 **Decitabine treatment abrogates the cisplatin-induced increase in %ALDH+ cells**

208 DNA hypomethylating agents like decitabine (DAC) have been shown to re-sensitize
209 platinum-resistant OC cells to platinum (33). Here, we used low dose DAC to determine the role
210 of DNA methylation in the cisplatin-induced changes observed above. Bisulfite sequencing of 12
211 CpG sites within the *BRCA1* promoter after DAC only and DAC +cisplatin dual treatment
212 confirmed that DAC treatment prevented the *BRCA1* promoter DNA hypermethylation caused by
213 cisplatin treatment alone (Supplementary Fig. S3, Fig. 4A). Corresponding to DAC blocking
214 platinum-induced *BRCA1* DNA hypermethylation (Fig. 2), dual treatment with DAC and cisplatin
215 resulted in significantly higher *BRCA1* expression levels than cisplatin treatment alone in both

OVCAR5 and OVSAHO cells, maintaining *BRCA1* levels at or above those in UT cells (Fig. 4B). With cisplatin treatment only, BRCA1 protein levels decreased (Fig. 4C; consistent with Fig. 1D). Importantly, BRCA1 protein levels were maintained after dual treatment of DAC and cisplatin to similar levels as UT cells (Fig. 4C). Unexpectedly, DAC treatment alone resulted in increased *BRCA1* expression and protein levels when compared to UT (Fig. 4B, C), suggesting that additional CpGs may be methylated at baseline in the *BRCA1* promoter than those interrogated or an indirect mechanism of DAC regulation of BRCA1 levels. Consistent with DNMT protein degradation in response to DAC treatment (34), DNMT1 and DNMT3B protein levels decreased in DAC treated cells with or without cisplatin treatment (Fig. 4C) and regardless of DAC treatment, γH2AX levels in cells treated with cisplatin increased as expected (Fig. 4C).

Next, the effect of low dose DAC on cisplatin-induced enrichment of OCSCs was determined. OVCAR5 cells treated with DAC had similar baseline %ALDH+ cells as UT while OVSAHO cells had significantly lower %ALDH+ cells than UT (Fig. 4D). As expected, cisplatin treatment increased in %ALDH+ cells in both cell lines and dual treatment with DAC and cisplatin blocked the cisplatin-induced increase in %ALDH+ cells with the %ALDH+ cells after dual treatment being similar to UT and/or DAC only treated cells (Fig. 4D).

To determine the role of low dose DAC and cisplatin dual treatment on OCSC survival, we examined the ability of pretreated cells to grow as spheroids in stem cell media. OVCAR5 and OVSAHO cells pretreated with cisplatin alone generated spheroids with increased viability compared to non-pretreated cells (4E; consistent with Fig. 1B). Spheroids derived from DAC pretreated only cells had similar viability as spheroids generated from non-pretreated cells (Fig. 4E). Dual pretreatment of DAC and cisplatin abrogated the cisplatin-induced spheroid formation

238 and increase in viable cells. Altogether, these data demonstrate that low dose DAC treatment
239 can prevent the platinum-induced enrichment of OCSCs, likely by maintaining BRCA1 expression.
240
241 **G2/M cell cycle arrest results in an increase %ALDH+ cells**
242 Because platinum induces cell cycle arrest (35), we studied if cell cycle arrest is related to
243 the cisplatin-induced enrichment of OCSCs. In UT OVCAR5 and OVSAHO cells, a higher percentage
244 of ALDH+ cells were in the G2/M phase of the cell cycle than ALDH- cells (OVCAR5: ALDH- = 4.4%,
245 ALDH+ = 15.3%, OVSAHO: ALDH - = 11.6%, ALDH+ = 34%) (Fig. 5A, Supplementary Fig. 4A). This
246 data is consistent with a prior study demonstrating a higher proportion of ALDH+ cells in G2/M
247 than ALDH- cells in other OC cell lines (35). Additionally, after treatment with cisplatin, there was
248 an expected increase in total cells in G2/M for both OVCAR5 ALDH- and ALDH+ cells (Fig. 5B;
249 ALDH+, 25.6% to 30.3%; ALDH-, 10.3% to 27.3%).
250 To determine if G2/M arrest is important for the cisplatin-induced increase in %ALDH+
251 cells (Fig. 1A), we induced G2/M arrest independent of platinum treatment through cyclin-
252 dependent kinase 1 inhibition (CDK1i) with the CDK inhibitor RO-3306 (36). CDK1 is a master
253 regulator of the cellular transition from G2 to M phase (37). CDK1i treatment increased the
254 percentage of cells in the G2/M phase of the cell cycle as compared UT and DMSO treatment to
255 a level that was similar to or higher than levels after cisplatin treatment in OVSAHO and OVCAR5
256 cells, respectively (Fig. 5C). Comparably to cisplatin, CDK1i treatment resulted in a significant
257 increase in %ALDH+ cells compared to UT in both cell lines (Fig. 5D). As a control for CDK1i
258 treatment, we determined total cells positive for phosphorylated Ser10 H3, a marker of active
259 mitosis. Compared to UT cells, there was a decrease in cells positive for phosphorylated Ser10

H3 after cisplatin and CDK1i treatments (UT: 2%, DMSO: 2.3%, cisplatin: 0.3% and CDK1i: 0.1%; Supplementary Fig. S4B); indicating G2/M arrest after cisplatin or CDK1i treatment, as expected. Additionally, unlike cisplatin treatment, CDK1i treatment did not induce DNA damage compared to UT as measured by γH2AX levels in OVCAR5 and OVSAHO cells (Supplementary Fig S4C), further supporting that G2/M arrest contributes to the cisplatin-induced increase in %ALDH+ cells.

NAMPT inhibition abrogates cisplatin-induced enrichment of ALDH+ cells

A key co-factor of ALDH activity is NAD^+ (38), and increased levels of NAD^+ and its rate-limiting regulator, NAMPT, have been shown to promote cancer cell survival and were associated with chemo-resistance and low patient survival (19, 39). Increased NAD^+ levels were also reported to drive a platinum-induced increase in senescence-associated OCSCs (23). We observed that NAD^+ levels were significantly higher in cells after 16 h of cisplatin treatment than in UT cells (Fig. 6A). In addition, *NAMPT* expression levels increased after 16 h acute cisplatin treatment suggesting that the cisplatin-induced increase in NAD^+ levels was due to a cisplatin-induced increase in *NAMPT* expression (Fig. 6B). Because the increase in *NAMPT* expression was highest after 16h cisplatin treatment, we determined *NAMPT* expression in OVSAHO, PEO1 and COV362 cell lines at this time point and observed similar cisplatin-induced increases in *NAMPT* expression (Fig. 6B and Supplementary Fig. S5). To determine if blocking the cisplatin-induced increase in NAD^+ prevented the increase in %ALDH+ cells, we treated cells with the NAMPT inhibitor- STF-118804 (NAMPTi), which has been shown to reduce cell viability in solid tumors (40). After cisplatin treatment with or without DMSO, NAD^+ levels increased compared to UT (Fig. 6C; consistent with Fig. 6A); furthermore, dual treatment with NAMPTi and cisplatin prevented

the cisplatin-induced increase in NAD^+ levels when compared to cisplatin treatment with or without DMSO and were similar to control levels or NAMPTi only (Fig. 6C).

Next, we examined the effect of dual treatment with NAMPTi and cisplatin on the cisplatin-induced increase in %ALDH+ cells. OVCAR5 cells treated with NAMPTi had decreased %ALDH+ cells relative to UT and DMSO treated cells, while OVSAHO NAMPTi treated cells had similar %ALDH+ cells as UT and DMSO treated cells (Fig. 6D). As expected, there was a significant increase in %ALDH+ cells after cisplatin treatment when compared to UT or DMSO treated cells in both cell lines. In contrast, dual treatment of NAMPTi and cisplatin prevented the cisplatin-induced increase in %ALDH+ cells, with the %ALDH+ cells in the dual treated samples being decreased or similar to levels in UT and DMSO treated cells in OVCAR5 and OVSAHO cells, respectively. Further, the effect of NAMPT inhibition on cisplatin-induced enrichment of OCSCs was investigated based on the ability of pretreated cells to grow as spheroids in stem cell media. As expected, cisplatin +DMSO pretreated cells were more spheroid like than UT and DMSO pretreated OVCAR5 cells (Fig. 6E, consistent with Fig. 1B). Spheroids viability after NAMPTi pretreatment was higher than DMSO pretreated cells but lower compared to cisplatin pretreated cells, and dual pretreatment with NAMPTi and cisplatin abrogated the cisplatin-induced spheroid formation and increase in viable cells (Fig. 6E). Additionally, dual pretreated cells had similar or lower viability as spheroids generated from DMSO or NAMPTi pretreated cells, respectively. These data demonstrate that cisplatin induced an increase in NAD^+ levels through increased expression of the rate-limiting enzyme, *NAMPT*, and NAMPT inhibition abrogated the cisplatin-induced enrichment of ALDH+ cells.

Cisplatin treatment induces two separate pathways to increase %ALDH+ cells

To further explore how decreased *BRCA1* expression, increased NAD^+ levels and G2/M arrest are interconnected during cisplatin-induced OCSC enrichment, we assayed *BRCA1* and *NAMPT* expression after CDK1 inhibition, BRCA1 overexpression and DAC treatment. In contrast to the cisplatin-induced decrease in *BRCA1* expression (Fig. 1C), *BRCA1* expression levels increased after CDK1i treatment in OVCAR5 and OVSAHO cells relative to UT and/or DMSO treated cells (Fig. 7A). However, consistent with the cisplatin treatment data, *NAMPT* RNA expression levels increased after CDK1i treatment in both cell lines compared to UT and/or DMSO treated cells (Fig. 7B). The level of NAMPT expression was higher in CDK1i compared to cisplatin treated OVSAHO cells (Fig. 7B).

These data suggest that G2/M cell cycle arrest and *NAMPT* expression but not *BRCA1* expression are connected, and to further confirm this relationship, we assayed *NAMPT* expression and NAD^+ levels in CpGi-null BRCA1 transfected cells, which we had previously demonstrated did not undergo cisplatin-induced enrichment of OCSC due to sustained BRCA1 expression (Fig. 3H). In EV and CpGi-null BRCA1 transfected OVCAR5 cells, *NAMPT* expression was elevated to a similar level relative to non-transfected UT cells and no further increase in NAMPT expression in transfected cells was observed after cisplatin treatment (Fig. 7C) even though, consistent with our previous results (Fig. 5B), cisplatin treatment increased *NAMPT* expression in non-transfected OVCAR5 cells. However, in OVSAHO cells, cisplatin treatment increased *NAMPT* expression in both EV and CpGi-null BRCA1 transfected cells compared to the UT transfected controls (Fig. 7C). In the absence of cisplatin treatment, *NAMPT* expression was similar in EV or CpGi-null BRCA1 transfected OVSAHO cells. Furthermore, CpGi-null BRCA1 transfected cells had

similar baseline NAD^+ levels as EV and non-transfected OVCAR5 cells (Fig. 7D) and NAD^+ levels increased after cisplatin treatment in non-transfected cells (Fig. 7D), as expected. Cisplatin treatment still increased NAD^+ levels in EV and CpGi-null BRCA1 transfected cells compared to UT controls although to a lesser extent than in non-transfected cells (Fig. 7D). This data suggests that even though maintaining BRCA1 expression blocks the cisplatin-induced increase in %ALDH+ cells, cisplatin treatment still increases NAD^+ levels.

BRCA1 overexpression has been previously connected to an increase of cells in the G2/M phase of the cell cycle (41). So, it was of interest to determine if changes in the cell cycle were driving the effect on platinum-induced OCSC enrichment when *BRCA1* expression was maintained by either CpGi-null transfection or DAC treatment. UT CpGi-null BRCA1 transfected cells had a higher percentage of cells in G2/M phase of the cell cycle when compared to UT non-transfected or EV transfected OVCAR5 cells (Supplementary Fig. 6). Cisplatin treatment of CpGi-null BRCA1 transfected cells increased total cells in G2/M phase of the cell cycle compared to cisplatin treated non-transfected cells and EV transfected cells as well as all types of UT cells. EV transfected cells treated with or without cisplatin had higher percentage of cells in G2/M phase of the cell cycle compared to UT non-transfected cells controls, which may explain the elevated *NAMPT* expression in these cells (Fig. 7C). Even though DAC treatment blocked the platinum-induced decrease in *BRCA1* expression (Fig. 4A) and increase in %ALDH+ cells (Fig. 4C), DAC treatment alone or in combination with cisplatin still elevated *NAMPT* expression compared to UT, and the level was similar to (or higher) than cells treated with cisplatin (Fig. 7E). Altogether, these data indicate that G2/M cell cycle arrest and the associated change in *NAMPT* expression were required for platinum-induced OCSC enrichment independently of decreased *BRCA1*

348 expression. Furthermore, our previous ATMi data indicated that DNA damage and/or the DDR
349 were required for the platinum-induced decrease in *BRCA1* expression and are separate from cell
350 cycle related changes in *NAMPT* expression.
351
352 **Dual DNMTi and NAMPTi treatment abrogate the cisplatin-induced increase in %ALDH+ cells**
353 The above observations indicated that both the cisplatin-induced decrease in BRCA1
354 levels and increase in *NAMPT* expression and NAD^+ levels were required for the platinum-induced
355 increase in %ALDH+ cells. Thus, two pathways contributed to the cisplatin-induced enrichment
356 of OCSCs, namely the DDR-linked decrease in BRCA1 expression and the cell cycle-linked increase
357 in *NAMPT* expression and NAD^+ levels. Although inhibiting either pathway alone with low
358 concentrations of DAC (Fig. 4) or NAMPTi (Fig. 6) abrogated the cisplatin-induced enrichment of
359 OCSC, we hypothesized that combining very low dose treatment of the two inhibitors would
360 impact both pathways and further abrogate the cisplatin-induced increase in %ALDH+ cells.
361 First, several concentrations of DAC and NAMPTi were used alone to determine doses of
362 each that had minimal to no effect on the cisplatin-induced increase in %ALDH+ cells (NAMPTi -
363 12.5 nM; DAC - 10 nM and 20 nM; Supplementary Fig. S7A, B). Then, we sought to determine if
364 combining selected lower doses of each drug would prevent the cisplatin-induced increase in
365 %ADLH+ cells. As expected, cells treated with individual very low dose DAC and low dose NAMPTi
366 in combination with cisplatin had similar increases in %ALDH+ cells as cells treated with cisplatin
367 alone in OVCAR5 and OVSAHO cells (Fig. 8A). Importantly, combination treatment of very low
368 dose DAC with low dose NAMPTi and cisplatin prevented the cisplatin-induced increase in
369 %ALDH+ cells and resulted in similar %ALDH+ cells as DMSO treated cells in both cell lines.

Furthermore, using Compusyn software (42) that uses combination index theorem, treatment of very low dose DAC (10 nM and 20 nM) with low dose NAMPTi and cisplatin synergistically inhibited (CI< 1) the cisplatin-induced increase in %ALDH+ cells in OVCAR5 cells (Fig. 8B). Whereas, in OVSAHO cells, very low dose DAC (10 nM) with low dose NAMPTi and cisplatin synergistically inhibited (CI < 1) the cisplatin-induced increase in %ALDH+ cells.

To confirm the effect of very low dose DAC and low dose NAMPT inhibition on cisplatin-induced enrichment of OCSCs, the ability of pretreated cells to grow as spheroids in stem cell media was examined. As expected, cisplatin pretreated cells were more spheroid-like compared to UT in both cell lines (Fig. 8C). Furthermore, cells pretreated with individual very low doses of DAC or low dose NAMPTi in combination with cisplatin pretreatment were similar to cisplatin pretreated cells (Fig. 8C; more spheroid-like and increased viability than UT). Importantly, combination pretreatment of very low dose DAC, low dose NAMPTi and cisplatin prevented cisplatin-induced spheroid formation and increase in viability. These data support the hypothesis that both pathways contribute to the cisplatin-induced enrichment of OCSCs.

Discussion

While HGSOC is initially highly responsive to chemotherapy, recurrence is common, and the majority of recurrent OC is chemotherapy resistant and fatal. OCSCs have increased resistance to chemotherapy and are enriched in OC relapses suggesting that OCSCs contribute to disease recurrence and resistance (4). Here we demonstrate that acute platinum treatment enriches the OCSC population, consistent with previous findings showing similar enrichment after

longer exposures to platinum (23, 43, 44). We identify two distinct pathways that drive chemotherapy-induced OCSC enrichment, one marked by reduced wildtype *BRCA1* expression and the other by increased NAD^+ levels. Blocking either pathway alone or inhibiting both pathways together by combining very low doses of specific inhibitors prevents acute platinum-induced OCSC enrichment in wildtype BRCA1, platinum-sensitive HGSOC. Our findings support using the novel combination treatment scheme as a neoadjuvant treatment to reduce the platinum-induced enrichment of ALDH+ OCSCs and to avert the development of platinum resistance.

BRCA1 is an OC susceptibility gene and *BRCA1* mutation increases the risk of developing OC (1). BRCA1 plays a role in ICL repair as well as other parts of the DDR (16). Additionally, ICL accumulation following BRCA1 depletion results in dedifferentiation of mammary epithelial cells to a more primitive, mesenchymal state (28). HGSOC accounts for approximately 70% of all EOC and the vast majority of patients diagnosed with HGSOC will have wildtype BRCA1. We demonstrate that platinum-induced a decrease in wildtype *BRCA1* expression that contributes to the observed enrichment of ALDH+ cells and concurrent increase in the CSC phenotype. Inhibiting ATM in combination with platinum blocked the platinum-induced decrease in *BRCA1* expression and OCSC enrichment demonstrating that the DDR after platinum treatment is important for the proposed mechanism. Consistent with the requirement for the DDR, stable BRCA1 knockdown without platinum treatment was not sufficient to increase the %ALDH+ cells. We speculate that the platinum-induced decrease in BRCA1 levels lead to persistent ICLs or alternative DNA repair pathway activation, which is required for but not sufficient for ALDH+ OCSC cell enrichment. Reduced BRCA1 levels may also contribute to senescence that occurs at later time-points post-

414 platinum, based on prior work demonstrating that alterations in BRCA1 after oncogene
415 expression precede and contribute to oncogene-induced senescence (45).

416 *BRCA1* expression can be regulated by many mechanisms, including promoter DNA
417 hypermethylation. Here we show that the cisplatin-induced decrease in BRCA1 levels correlated
418 with an increase in *BRCA1* promoter DNA hypermethylation. Uniquely, we demonstrated that
419 combining treatment with the DNMT inhibitor DAC with cisplatin blocks the cisplatin-induced
420 increase in %ALDH+ cells and spheroid formation. Both DAC treatment and expression of CpGi-
421 null BRCA1, which also blocked the platinum-induced OCSC enrichment, maintained *BRCA1*
422 expression levels at or above the levels of untreated cells even after cisplatin treatment. These
423 findings lead us to suggest that there is a "threshold effect" for BRCA1 levels: BRCA1 levels at or
424 above baseline prevent enrichment of ALDH+ cells, and OCSC enrichment occurs when BRCA1
425 levels fall below baseline in the presence of an activated DDR.

426 In addition to the DDR-dependent changes in *BRCA1* expression, we have reported that a
427 parallel pathway exists where platinum induces an increase in NAD^+ levels, and altering this
428 metabolic pathway is also required for platinum-induced OCSC enrichment. Metabolic pathways
429 have been shown to contribute to platinum resistance (44). NAD^+ is a cofactor of ALDH enzymes
430 that catalyze the oxidation of aldehydes (21) and are overexpressed in OCSCs. We demonstrated
431 that elevated levels of NAD^+ correspond to the timing of ALDH+ cell enrichment. Because NAD^+
432 is a cofactor for ALDH, the platinum-induced increase in cellular NAD^+ levels likely drives the
433 increased ALDH activity of OCSCs. Furthermore, inhibition of NAMPT, the rate limiting enzyme
434 for NAD^+ synthesis from the salvage pathway, blocked the cisplatin-induced enrichment of ALDH+
435 cells. These findings are consistent with a recent study linking platinum exposure to increased

436 *NAMPT* expression and NAD^+ levels that are required for platinum-induced senescence-
437 associated enrichment of OCSCs (23). However, we report that these changes occur a very early
438 point post platinum (16 h versus 4 days) and at 16 h we do not observe indicators of senescence
439 such as changes in *HMGA1* expression (data not shown), suggesting that our observed increases
440 in *NAMPT* expression, NAD^+ levels and OCSC enrichment occur before and perhaps contribute to
441 platinum-induced senescent phenotypes. Our studies combined with Nacarelli et al. support
442 further preclinical and clinical studies aimed at investigating NAMPT inhibition as a potential
443 therapeutic strategy to prevent the development of platinum resistant OC.

444 Loss of BRCA1 induces metabolic reprogramming through the Nicotinamide N-
445 methyltransferase (NNMT) pathway in OC cells (46). We show that the platinum-induced
446 decrease in BRCA1 levels occurs concomitantly with increased NAD^+ levels. NNMT is also involved
447 in NAD^+ synthesis. NNMT transfers methyl group from S-adenosyl methionine (SAM) to
448 nicotinamide (NAM) resulting in 1-methylnicotinamide (MNA) during the conversion of SAM to
449 S-adenosyl-L-homocysteine (SAH). In the NAD^+ salvage pathway, NAMPT uses NAM as a
450 substrate, ultimately resulting in the production of NAD^+ (19). Therefore, we hypothesized that
451 the decrease in *BRCA1* expression and increase in NAD^+ levels may be mechanistically connected.
452 However, even though expression of *BRCA1* in cells transfected with CpGi-null BRCA1 blocks the
453 platinum-induced increase in %ALDH+ cells, NAD^+ levels still increase in these cells (Fig. 7D).
454 Importantly, in *BRCA1* mutant HGSOC COV362 cells, cisplatin-induced an increase in *NAMPT*
455 expression but no enrichment of ALDH+ cells. However, as mentioned, inhibition of NAMPT was
456 sufficient to block the platinum-induced increase in %ALDH+ cells. We suggest that the platinum-
457 induced decrease in BRCA1 and increase in *NAMPT* and NAD^+ levels occur as part of distinct

parallel pathways which independently contribute to platinum-induced OCSC enrichment. Future studies will further investigate how these platinum-induced DDR and metabolic alterations result in OCSC enrichment.

Cellular NAD^+ is produced primarily in G1 and G2 cell cycle phases (47) and CDK1 inhibition has been shown to promote the nuclear localization of NAMPT to replenish decreased NAD^+ levels after CDK1 inhibitor treatment (48). We show that inhibiting CDK1 induces OCSC enrichment that is associated with an increase in *NAMPT* expression (Fig. 7B) but not a decrease in *BRCA1* expression (Fig. 7A), providing support for the hypothesis that the platinum-induced increase in *NAMPT* expression and NAD^+ levels are driven by cell cycle changes independent of changes in *BRCA1* expression. In response to DNA damage, BRCA1 is a part of a complex that initiates G2/M arrest to allow time for DNA damage repair (49). Consistent with this role, CpGi-null BRCA1 transfection increases the percentage of cells in the G2/M phase of cell cycle both with and without cisplatin treatment (Supplementary Fig. 6A). Interestingly, further connecting G2/M and NAD^+ levels, platinum-treated, CpGi-null BRCA1 transfected cells have elevated NAD^+ levels but are not enriched for OCSCs (Fig. 7D, (41)). Together these findings suggest that G2/M arrest leads to increased *NAMPT* expression and NAD^+ levels that contribute to OCSC enrichment; however, after platinum treatment, these changes must occur in conjunction with decreased levels of BRCA1, otherwise OCSC enrichment will be blocked. These data also demonstrate that the effect of BRCA1 overexpression on platinum-induced OCSC enrichment is independent of its effect on cell cycle.

Clinically, DNMT inhibitors have been used to re-sensitize chemoresistant OC cells to chemotherapy (33, 50-53). Our study extends these findings by demonstrating that DNMT

480 inhibitors may also be beneficial when used in combination with neoadjuvant/adjuvant
481 chemotherapy in OC patients where they have the potential to block platinum-induced OCSC
482 enrichment and establishment of platinum resistance. NAMPT inhibitors like FK866 and
483 GMX1778 have been shown to have preclinical antitumor efficacy *in vivo* by suppressing
484 chemoresistant senescence-associated enrichment of OCSCs (23). NAMPT inhibitors have also
485 been clinically tested in advanced hematological and solid malignancies (54, 55). However, dose
486 limiting toxicities were a significant problem and objective tumor remission was not observed.
487 Even the currently used "low doses" of DNMT inhibitors still result in dose-limiting toxicities and
488 adverse advents (52, 53). Importantly, we demonstrate that the combination of very low dose
489 DNMT inhibitors with low dose metabolic inhibitors provides an effective treatment scheme to
490 prevent onset of platinum resistance in OC. Using lower concentrations of these inhibitors may
491 reduce off-target cytotoxic effects and make the treatment more tolerable to patients.
492
493 **Methods and Materials**
494 **Cell lines, culture conditions, and reagents**
495 Epithelial OC cell lines OVCAR5, OVCAR3, COV362, OVSAHO and PEO1 were maintained at 37°C
496 and 5% CO_2 humidified atmosphere using standard conditions (24, 25, 56). All cell lines were
497 tested for mycoplasma in 2017 (ATCC, 30-1012K). For all treatments, 1 million cells were plated
498 in a 100 mm^2 dish and treated the next day for the specified number of hours. Cisplatin (EMD
499 Millipore, 232120) was dissolved in 154 mM NaCl at 1.67 nM, filter sterilized and stored at 4 °C.
500 Cells were treated with cell line specific IC_{50} dose of cisplatin (OVCAR5: 12.00 μM, OVSAHO: 4.00
501 μM, OVCAR3, 15.00 μM, PEO1: 12.84 μM, COV362: 13.57 μM) (24). CDK1 inhibitor (Sigma-

Aldrich, SML0569) was dissolved in DMSO and stored (-20 °C, 10 mM stock solution). Decitabine (Sigma, A3656) was solubilized in dH_2O and stored (-80 °C, 2 μg/μL stock solution). Cells were treated with CDK1i (9 μM for 16 h) or DAC (100 nM for 48 h). Media containing fresh DAC was changed every 24 h. Cisplatin was added during the last 16 h of DAC treatment. NAMPT inhibitor (Sigma-Aldrich, SML1348) was dissolved in DMSO and stored (4 °C, 10 mM stock solution). Cells were treated with NAMPTi (50 nM for 6h). For cisplatin and NAMPTi dual treatment, cells were treated with cisplatin as mentioned above, then NAMPTi was added 10 h later. For low dose NAMPTi and DAC combination treatment with cisplatin, cells were treated with DAC (10 nM or 20 nM for 48 h), cisplatin was added in the last 16 h and NAMPTi (12.5 nM) was added during the last 6 h of the DAC treatment. ATM inhibitor KU-55933 (Sigma, MO #SML1109) was dissolved in DMSO and stored (-20 °C, 10 mM stock solution). Cells were treated with 15 μM ATMi for 16 h in combination with cisplatin.

ALDEFLUOR assay and flow cytometry

ALDH activity was measured through ALDEFLUOR assay (Stem Cell technologies, 01700). Cultured cells were trypsinized, washed with 1X PBS and 1 million cells were resuspended in 1 mL ALDEFLUOR assay buffer containing substrate, bodipyaminoacetaldehyde (BAAA). Next, 0.5 mL of resuspended mixture was moved to another tube containing ALDH inhibitor, 5 μL 1.5 mM diethylamino benzaldehyde (DEAB). These solutions were incubated for 30-40 min at 37 °C in the dark. After incubation, cells were centrifuged and resuspended in fresh ALDEFLUOR assay buffer and filtered through a 30 μm filter (Sysmex).

Flow cytometry analysis was performed on a LSRII flow cytometer (BD Biosciences) at IU Flow Cytometry Core Facility. ALDH activity was measured using 488 nm excitation and the signal was detected using the 530/30 filter and analyzed at least three times in independent experiments. For each experiment, 10,000 events were analyzed. ALDH+ percentage gate was determined by sample specific negative control (DEAB) ALDH+ gate. Further data analysis was done in FlowJo software (Becton, Dickinson & Company).

Cell cycle analysis

Nuclear-ID red DNA stain (Enzo Life Sciences, ENZ-52406) was used to analyze cell cycle to allow for combination with the ALDFLUOR assay, which requires live cells. After treatment with cisplatin, cells were trypsinized and resuspended in 1X PBS. Then, 1:250 dilution of Nuclear-ID red DNA stain was added to the total volume and solution was incubated for 30 min at 37 °C in the dark. To determine cell cycle profile for ALDH+ population, cells were first suspended with ALDEFLUOR reagent and incubated for 30 min at 37 °C, followed by Nuclear-ID stain as above and then, analyzed by flow cytometry using the LSRII. Nuclear ID was excited at 561 nm and detected using the 670/30 filter and analyzed at least three times in independent experiments. For each experiment, 10,000 events were analyzed. FlowJo software was used for data analysis.

Quantitative RT-PCR (qRT-PCR)

Total RNA was isolated from cell pellets using RNeasy Mini Kit (Qiagen, 74104) and cDNA was generated using Maxima First Strand cDNA Synthesis Kit for RT-qPCR (Thermo Fisher Scientific, K1642). qPCR was done on a LightCycler 96 using TaqMan MasterMix (Thermo Fisher,

04535286001) or FastStart Essential DNA Green Master (Roche, 06402712001). C_q values for genes of interest were normalized to housekeeping genes (*PPIA*, *β-Actin or RhoA*) using the deltaCq method. Detailed information for primers can be found in Supplementary Table S1.

DNA extraction, bisulfite conversion, qMSP and bisulfite sequencing

DNA was extracted from cell pellets using the DNeasy Blood and Tissue Kit (Qiagen, 69504) and bisulfite treated using the EZ DNA Methylation-Gold kit (Zymo Research, D5006). For qMSP, methods were followed as described in a previous publication (57). qMSP primers used are listed in supplementary methods table S1. For bisulfite sequencing, bisulfite converted DNA was amplified using AmpliTaq Gold 360 Mastermix (ThermoFisher Scientific, 4398881) using primers listed in the supplementary methods table S1. Then, the amplified product was run on an agarose gel, the correct band was excised from the gel, and DNA was purified using the QIAquick Gel Extraction kit (Qiagen, 28704). The DNA was then cloned into One Shot™ TOP10 Chemically Competent *E. coli* using the TOPO™ TA Cloning™ Kit for Sequencing (ThermoFisher Scientific, 451641). The next day, white colonies were inoculated in LB+ carbenicillin media overnight and plasmid was extracted using Zyppy Plasmid Miniprep Kit (Zymo research, D4020) and sequenced by Sanger sequencing. Sequence peaks were analyzed for good quality in 4peaks software and DNA methylation maps were generated through BioAnalyzer (Max-Planck-Institute for Informatics and Saarland University, Saarbrücken, Germany) (58).

Western blot analysis

Cell pellets were lysed in 4% SDS buffer using a QIAshredder (Qiagen, 79654). After protein was extracted, western blotting was performed. Antibodies used are listed in supplementary methods. Band density was measured by ImageJ software (NIH) and normalized to laminB, β -actin or vimentin.

Spheroid formation assay

1.5×10^4 cells pre-treated with cisplatin (6 μM for 3 h), NAMPTi (50 nM for 6 h), and/or DAC (100 nM for 48 h) were plated in a 24-well low attachment plate (Corning, 3473) containing stem cell media (43) for 14 days. Media was added every 3 days to each well. On day 14, images were taken using an EVOS FL Auto microscope (Life Technologies). Then, cell viability reagent (Abcam, ab176748), which measures cell viability be intracellular esterase activity, was added directly to each spheroid well at a volume equal to the volume of media in the well. After 1 h incubation, the reagent+ media solution was distributed in an opaque 96-well plate. Viability (Ex/Em: 405/460 nm) was measured using a SynergyH1 plate reader (BioTek). The experiment was done in 4 technical replicates for each condition.

NAD^+/NADH ratio

NAD^+/NADH ratio was calculated using NAD^+/NADH quantification colorimetric kit (BioVision, K337-100) according to the manufacturer's instructions.

Transfection

1 million cultured cells were transfected with plasmid using Turbofect (ThermoFisher Scientific, R0532) 48 h before treatment and then cells were collected. pBABEpuro HA-BRCA1 was a gift from Stephen Elledge (Addgene plasmid # 14999; http://n2t.net/addgene:14999; RRID:Addgene_14999) (59). pBABE-puro was a gift from Hartmut Land, Jay Morgenstern and Bob Weinberg (Addgene plasmid # 1764; http://n2t.net/addgene:1764 ; RRID:Addgene_1764) (60).

Viral shRNA knockdown preparation and stable cell line knockdown generation

For BRCA1 knockdown, shRNA1 (Sigma, TRCN0000244986) and shRNA2 (Sigma, TRCN0000244984) and empty vector (EV) TRC2 (Sigma, SHC201) were used and lentiviral shRNA was created following the protocol as previously described (56). For cell line infection, 2 x 10^5 cells/mL were plated and after 24 h, virus was added in media with polybrene. Puromycin was added 24 h post-viral infection and cells were plated for downstream experiments once confluent.

Statistical methods

All experiments were performed in at least three biological replicates. When two groups were compared, statistical comparison was performed by Student's t-test. One-way ANOVA followed by Tukey post hoc test was used to compare multiple groups using Graphpad Prism.

References:

1. Siegel RL, Miller KD, Jemal A. Cancer Statistics, 2017. *CA Cancer J Clin* **67**, 7-30, (2017)

608 2. Torre LA, Trabert B, DeSantis CE, Miller KD, Samimi G, Runowicz CD, et al. Ovarian
609 cancer statistics, 2018. *CA Cancer J Clin* **68**, 284-296, (2018)
610 3. Matulonis UA, Sood AK, Fallowfield L, Howitt BE, Sehouli J, Karlan BY. Ovarian cancer.
611 *Nat Rev Dis Primers* **2**, 16061, (2016)
612 4. Wang Y, Cardenas H, Fang F, Condello S, Taverna P, Segar M, et al. Epigenetic targeting
613 of ovarian cancer stem cells. *Cancer Res* **74**, 4922-4936, (2014)
614 5. Roy L, Cowden Dahl KD. Can Stemness and Chemoresistance Be Therapeutically
615 Targeted via Signaling Pathways in Ovarian Cancer? *Cancers (Basel)* **10**, (2018)
616 6. Lupia M, Cavallaro U. Ovarian cancer stem cells: still an elusive entity? *Mol Cancer* **16**,
617 64, (2017)
618 7. Silva IA, Bai S, McLean K, Yang K, Griffith K, Thomas D, et al. Aldehyde dehydrogenase in
619 combination with CD133 defines angiogenic ovarian cancer stem cells that portend poor
620 patient survival. *Cancer Res* **71**, 3991-4001, (2011)
621 8. Lobo NA, Shimono Y, Qian D, Clarke MF. The biology of cancer stem cells. *Annu Rev Cell*
622 *Dev Biol* **23**, 675-699, (2007)
623 9. Chaney SG, Campbell SL, Bassett E, Wu Y. Recognition and processing of cisplatin- and
624 oxaliplatin-DNA adducts. *Crit Rev Oncol Hematol* **53**, 3-11, (2005)
625 10. Maugeri-Sacca M, Bartucci M, De Maria R. DNA damage repair pathways in cancer stem
626 cells. *Mol Cancer Ther* **11**, 1627-1636, (2012)
627 11. Wagner JM, Karnitz LM. Cisplatin-induced DNA damage activates replication checkpoint
628 signaling components that differentially affect tumor cell survival. *Mol Pharmacol* **76**, 208-214,
629 (2009)

12. Abdullah LN, Chow EK. Mechanisms of chemoresistance in cancer stem cells. *Clin Transl Med* **2**, 3, (2013)

13. Venkitaraman AR. Functions of BRCA1 and BRCA2 in the biological response to DNA damage. *J Cell Sci* **114**, 3591-3598, (2001)

14. Pathania S, Nguyen J, Hill SJ, Scully R, Adelmant GO, Marto JA, et al. BRCA1 is required for postreplication repair after UV-induced DNA damage. *Mol Cell* **44**, 235-251, (2011)

15. Silver DP, Livingston DM. Mechanisms of BRCA1 tumor suppression. *Cancer Discov* **2**, 679-684, (2012)

16. Roy R, Chun J, Powell SN. BRCA1 and BRCA2: different roles in a common pathway of genome protection. *Nat Rev Cancer* **12**, 68-78, (2011)

17. Maxwell KN, Wubbenhorst B, Wenz BM, De Sloover D, Pluta J, Emery L, et al. BRCA locus-specific loss of heterozygosity in germline BRCA1 and BRCA2 carriers. *Nat Commun* **8**, 319, (2017)

18. Chiang JW, Karlan BY, Cass L, Baldwin RL. BRCA1 promoter methylation predicts adverse ovarian cancer prognosis. *Gynecol Oncol* **101**, 403-410, (2006)

19. Yaku K, Okabe K, Hikosaka K, Nakagawa T. NAD Metabolism in Cancer Therapeutics. *Front Oncol* **8**, 622, (2018)

20. Hayes K, Noor M, Djeghader A, Armshaw P, Pembroke T, Tofail S, et al. The quaternary structure of Thermus thermophilus aldehyde dehydrogenase is stabilized by an evolutionary distinct C-terminal arm extension. *Sci Rep* **8**, 13327, (2018)

650 21. Liu ZJ, Sun YJ, Rose J, Chung YJ, Hsiao CD, Chang WR, et al. The first structure of an
651 aldehyde dehydrogenase reveals novel interactions between NAD and the Rossmann fold. *Nat*
652 *Struct Biol* **4**, 317-326, (1997)
653 22. Li D, Chen NN, Cao JM, Sun WP, Zhou YM, Li CY, et al. BRCA1 as a nicotinamide adenine
654 dinucleotide (NAD)-dependent metabolic switch in ovarian cancer. *Cell Cycle* **13**, 2564-2571,
655 (2014)
656 23. Nacarelli T, Fukumoto T, Zundell JA, Fatkhutdinov N, Jean S, Cadungog MG, et al. NAMPT
657 Inhibition Suppresses Cancer Stem-like Cells Associated with Therapy-Induced Senescence in
658 Ovarian Cancer. *Cancer Res* **80**, 890-900, (2020)
659 24. Haley J, Tomar S, Pulliam N, Xiong S, Perkins SM, Karpf AR, et al. Functional
660 characterization of a panel of high-grade serous ovarian cancer cell lines as representative
661 experimental models of the disease. *Oncotarget* **7**, 32810-32820, (2016)
662 25. Pulliam N, Fang F, Ozes AR, Tang J, Adewuyi A, Keer H, et al. An Effective Epigenetic-
663 PARP Inhibitor Combination Therapy for Breast and Ovarian Cancers Independent of BRCA
664 Mutations. *Clin Cancer Res* **24**, 3163-3175, (2018)
665 26. Mitra AK, Davis DA, Tomar S, Roy L, Gurler H, Xie J, et al. In vivo tumor growth of high-
666 grade serous ovarian cancer cell lines. *Gynecol Oncol* **138**, 372-377, (2015)
667 27. Tomita H, Tanaka K, Tanaka T, Hara A. Aldehyde dehydrogenase 1A1 in stem cells and
668 cancer. *Oncotarget* **7**, 11018-11032, (2016)
669 28. Wang H, Bierie B, Li AG, Pathania S, Toomire K, Dimitrov SD, et al.
670 BRCA1/FANCD2/BRG1-Driven DNA Repair Stabilizes the Differentiation State of Human
671 Mammary Epithelial Cells. *Mol Cell* **63**, 277-292, (2016)

672 29. Kondrashova O, Topp M, Nesic K, Lieschke E, Ho GY, Harrell MI, et al. Methylation of all
673 BRCA1 copies predicts response to the PARP inhibitor rucaparib in ovarian carcinoma. *Nat*
674 *Commun* **9**, 3970, (2018)
675 30. Greenberg MVC, Bourc'his D. The diverse roles of DNA methylation in mammalian
676 development and disease. *Nat Rev Mol Cell Biol* **20**, 590-607, (2019)
677 31. Daley JM, Sung P. 53BP1, BRCA1, and the choice between recombination and end
678 joining at DNA double-strand breaks. *Mol Cell Biol* **34**, 1380-1388, (2014)
679 32. Podhorecka M, Skladanowski A, Bozko P. H2AX Phosphorylation: Its Role in DNA
680 Damage Response and Cancer Therapy. *J Nucleic Acids* **2010**, (2010)
681 33. Fang F, Balch C, Schilder J, Breen T, Zhang S, Shen C, et al. A phase 1 and
682 pharmacodynamic study of decitabine in combination with carboplatin in patients with
683 recurrent, platinum-resistant, epithelial ovarian cancer. *Cancer* **116**, 4043-4053, (2010)
684 34. Yu J, Qin B, Moyer AM, Nowsheen S, Liu T, Qin S, et al. DNA methyltransferase
685 expression in triple-negative breast cancer predicts sensitivity to decitabine. *J Clin Invest* **128**,
686 2376-2388, (2018)
687 35. Bellio C, DiGloria C, Foster R, James K, Konstantinopoulos PA, Growdon WB, et al. PARP
688 Inhibition Induces Enrichment of DNA Repair-Proficient CD133 and CD117 Positive Ovarian
689 Cancer Stem Cells. *Mol Cancer Res* **17**, 431-445, (2019)
690 36. Vassilev LT. Cell cycle synchronization at the G2/M phase border by reversible inhibition
691 of CDK1. *Cell Cycle* **5**, 2555-2556, (2006)
692 37. Hochegger H, Takeda S, Hunt T. Cyclin-dependent kinases and cell-cycle transitions:
693 does one fit all? *Nat Rev Mol Cell Biol* **9**, 910-916, (2008)

694 38. Perez-Miller SJ, Hurley TD. Coenzyme isomerization is integral to catalysis in aldehyde
695 dehydrogenase. *Biochemistry* **42**, 7100-7109, (2003)
696 39. Kennedy BE, Sharif T, Martell E, Dai C, Kim Y, Lee PW, et al. NAD(+) salvage pathway in
697 cancer metabolism and therapy. *Pharmacol Res* **114**, 274-283, (2016)
698 40. Espindola-Netto JM, Chini CCS, Tarrago M, Wang E, Dutta S, Pal K, et al. Preclinical
699 efficacy of the novel competitive NAMPT inhibitor STF-118804 in pancreatic cancer. *Oncotarget*
700 **8**, 85054-85067, (2017)
701 41. Wang L, Zeng X, Chen S, Ding L, Zhong J, Zhao JC, et al. BRCA1 is a negative modulator of
702 the PRC2 complex. *EMBO J* **32**, 1584-1597, (2013)
703 42. Chou TC. Drug combination studies and their synergy quantification using the Chou-
704 Talalay method. *Cancer Res* **70**, 440-446, (2010)
705 43. Wang Y, Zong X, Mitra S, Mitra AK, Matei D, Nephew KP. IL-6 mediates platinum-induced
706 enrichment of ovarian cancer stem cells. *JCI Insight* **3**, (2018)
707 44. Matassa DS, Amoroso MR, Lu H, Avolio R, Arzeni D, Procaccini C, et al. Oxidative
708 metabolism drives inflammation-induced platinum resistance in human ovarian cancer. *Cell*
709 *Death Differ* **23**, 1542-1554, (2016)
710 45. Tu Z, Aird KM, Bitler BG, Nicodemus JP, Beeharry N, Xia B, et al. Oncogenic RAS regulates
711 BRIP1 expression to induce dissociation of BRCA1 from chromatin, inhibit DNA repair, and
712 promote senescence. *Dev Cell* **21**, 1077-1091, (2011)
713 46. Kanakkanthara A, Kurmi K, Ekstrom TL, Hou X, Purfeerst ER, Heinzen EP, et al. BRCA1
714 Deficiency Upregulates NNMT, Which Reprograms Metabolism and Sensitizes Ovarian Cancer
715 Cells to Mitochondrial Metabolic Targeting Agents. *Cancer Res* **79**, 5920-5929, (2019)

716 47. Yu FX, Dai RP, Goh SR, Zheng L, Luo Y. Logic of a mammalian metabolic cycle: an
717 oscillated NAD+/NADH redox signaling regulates coordinated histone expression and S-phase
718 progression. *Cell Cycle* **8**, 773-779, (2009)
719 48. Svoboda P, Krizova E, Sestakova S, Vapenkova K, Knejzlik Z, Rimpelova S, et al. Nuclear
720 transport of nicotinamide phosphoribosyltransferase is cell cycle-dependent in mammalian
721 cells, and its inhibition slows cell growth. *J Biol Chem* **294**, 8676-8689, (2019)
722 49. Lobrich M, Jeggo PA. The impact of a negligent G2/M checkpoint on genomic instability
723 and cancer induction. *Nat Rev Cancer* **7**, 861-869, (2007)
724 50. Fang F, Zuo Q, Pilrose J, Wang Y, Shen C, Li M, et al. Decitabine reactivated pathways in
725 platinum resistant ovarian cancer. *Oncotarget* **5**, 3579-3589, (2014)
726 51. Matei D, Fang F, Shen C, Schilder J, Arnold A, Zeng Y, et al. Epigenetic resensitization to
727 platinum in ovarian cancer. *Cancer Res* **72**, 2197-2205, (2012)
728 52. Matei D, Ghamande S, Roman L, Alvarez Secord A, Nemunaitis J, Markham MJ, et al. A
729 Phase I Clinical Trial of Guadecitabine and Carboplatin in Platinum-Resistant, Recurrent Ovarian
730 Cancer: Clinical, Pharmacokinetic, and Pharmacodynamic Analyses. *Clin Cancer Res* **24**, 2285-
731 2293, (2018)
732 53. Oza AM, Matulonis UA, Alvarez Secord A, Nemunaitis J, Roman LD, Blagden SP, et al. A
733 Randomized Phase II Trial of Epigenetic Priming with Guadecitabine and Carboplatin in
734 Platinum-resistant, Recurrent Ovarian Cancer. *Clin Cancer Res* **26**, 1009-1016, (2020)
735 54. Holen K, Saltz LB, Hollywood E, Burk K, Hanauske AR. The pharmacokinetics, toxicities,
736 and biologic effects of FK866, a nicotinamide adenine dinucleotide biosynthesis inhibitor. *Invest*
737 *New Drugs* **26**, 45-51, (2008)

738 55. von Heideman A, Berglund A, Larsson R, Nygren P. Safety and efficacy of NAD depleting
739 cancer drugs: results of a phase I clinical trial of CHS 828 and overview of published data.
740 *Cancer Chemother Pharmacol* **65**, 1165-1172, (2010)
741 56. Sriramkumar S, Matthews TD, Ghobashi AH, Miller SA, VanderVere-Carozza PS,
742 Pawelczak KS, et al. Platinum-Induced Ubiquitination of Phosphorylated H2AX by RING1A Is
743 Mediated by Replication Protein A in Ovarian Cancer. *Mol Cancer Res* **18**, 1699-1710, (2020)
744 57. Maiuri AR, Peng M, Podicheti R, Sriramkumar S, Kamplain CM, Rusch DB, et al. Mismatch
745 Repair Proteins Initiate Epigenetic Alterations during Inflammation-Driven Tumorigenesis.
746 *Cancer Res* **77**, 3467-3478, (2017)
747 58. Bock C, Reither S, Mikeska T, Paulsen M, Walter J, Lengauer T. BiQ Analyzer:
748 visualization and quality control for DNA methylation data from bisulfite sequencing.
749 *Bioinformatics* **21**, 4067-4068, (2005)
750 59. Cortez D, Wang Y, Qin J, Elledge SJ. Requirement of ATM-dependent phosphorylation of
751 brca1 in the DNA damage response to double-strand breaks. *Science* **286**, 1162-1166, (1999)
752 60. Morgenstern JP, Land H. Advanced mammalian gene transfer: high titre retroviral
753 vectors with multiple drug selection markers and a complementary helper-free packaging cell
754 line. *Nucleic Acids Res* **18**, 3587-3596, (1990)

755

756 **Acknowledgments**

757 We thank the Indiana University Flow Cytometry Core Facility for their assistance.

758

759 **Conflict of Interest Statement**: The authors declare no competing interests.

760

761 **Author Contribution Statement:**

762 R.S., K.P.N. and H.O.H performed study concept and design; R.S. and H.O.H. performed
763 development of methodology and writing; R.S, C.H., K.P.N., H.O.H., S.S. performed review and
764 revision of paper; R.S., S.K. and S.S. provided acquisition, analysis and interpretation of data and
765 statistical analysis; C.H. provided technical and material support

766

767 **Ethics statement:** Study did not require ethical approval

768

769 **Funding statement:** This research was funded by Ovarian Cancer Research Alliance grant
770 number 458788 to HMOH and KPN and in part through the IU Simon Cancer Center P30
771 Support Grant (P30CA082709). SS was supported by the Doane and Eunice Dahl Wright
772 Fellowship generously provided by Ms. Imogen Dahl.

773

774 **Figure Legends:**

775 **Fig 1. Cisplatin treatment enriches for ALDH+ cells.** A) %ALDH+ cells determined using the
776 ALDEFLUOR assay after mock (UT) or cisplatin (IC50 dose) treatment for the indicated time points.
777 N=3. **B)** Images of spheroids after mock (UT) or cisplatin (3 h, ½ IC50) pretreatment in indicated
778 cell lines. Scale bar = 500 μm. Graph depicts fluorescence intensity (RFU) of CytoCalcein Violet
779 450 stain. N=4. **C)** Relative *BRCA1* RNA expression in indicated cell lines after mock (UT) or
780 cisplatin treatment (16 h, IC50) for the indicated time points and cell lines. N=3. **B)** Western blot
781 and relative densitometry of whole cell lysates after mock (UT) or cisplatin (16 h, IC50) treatment

for the indicated time points and cell lines. N=3. For all panels, graphs indicate mean +/- SEM, *P<0.05, **P<0.001, ***P<0.0001, ****P<0.00001.

Fig 2. Cisplatin-induced decrease in *BRCA1* levels is associated with promoter DNA hypermethylation. A) Quantitative MSP for *BRCA1* promoter DNA methylation. Graphs depict mean + SEM. N=3. **B)** The location and methylation status of CpG sites in promoter region of *BRCA1* gene. Location of qMSP primers are indicated. The arrow at the transcription start site (TSS) indicates transcription direction. Individual CpG dinucleotides are shown as circles with closed circles: methylation and open circles: unmethylated. Sequencing of ten individual clones for each sample was performed from bisulfite-converted mock (UT) or cisplatin (16H, IC50) treated DNA. **C)** Percentage of methylated CpGs per clone using data presented in B. Graphs depict mean + SEM. N=10. **D)** Western blot of OVCAR5 whole cell lysates after mock (UT) or cisplatin (IC50 dose) treatment for the indicated time points. For all panels *P<0.05, **P<0.001, ***P<0.0001.

Fig 3. The cisplatin-induced decrease in BRCA1 is required for the associated increase in %ALDH+ cells. A) Relative *BRCA1* RNA expression in OVCAR5 cells after stable lentiviral infection with mock (EV) or BRCA1 shRNA1/2 with or without cisplatin treatment (16 h, IC50). Graphs depict mean + SEM. N=3. **B)** Western blot and relative densitometry of OVCAR5 whole cell lysates after mock (EV) with or without cisplatin treatment (16 h, IC50) or BRCA1 shRNA1/2. N=3. **C)** Percentage of ALDH+ cells using the ALDEFLUOR assay after stable lentiviral infection with mock (EV) with or without cisplatin treatment (16 h, IC50) or BRCA1 shRNA1/2. N=3. **D)** Relative *BRCA1*

804 RNA expression in indicated cell lines after mock (DMSO), cisplatin treatment (16 h, IC50), ATMi
805 (16 h, 152 μM) or ATMi (16 h, 152 μM) + cisplatin (16 h, IC50). N=3. **E)** Percentage of ALDH+ cells
806 using the ALDEFLUOR assay in indicated cell lines treated as in D. N=3. **F)** Relative *BRCA1* RNA
807 expression in cells transfected with mock empty vector (EV) or CpGi-null BRCA1 plasmid and
808 treated with or without cisplatin (16 h, IC50) in the indicated cell lines. N=3. **G)** Western blot and
809 relative densitometry of OVCAR5 whole cell lysates transfected and treated as in F. N=3. **H)**
810 Percentage of ALDH+ cells using the ALDEFLUOR assay after transfection with mock empty vector
811 (EV) or CpGi-null BRCA1 (BRCA1) plasmid and treatment as in F in indicated cell lines. N=3. For all
812 panels, graphs indicate mean +/- SEM, **P*<0.05, ***P*<0.001, ****P*<0.0001.
813
814 **Fig 4. Decitabine treatment abrogates the cisplatin induced increase in %ALDH+ cells. A)** The
815 location and methylation status of CpG sites in the BRCA1 promoter from bisulfite-converted
816 mock (UT), cisplatin treatment (16 h, IC50), DAC (48 h, 100 nM) or DAC (48 h, 100 nM) + cisplatin
817 (16 h, IC50) treated DNA. Closed circles: methylation and open circles: unmethylated. Sequencing
818 of ten individual clones for each sample was performed. **B)** Relative *BRCA1* RNA expression after
819 treatment as in A in indicated cell lines. N=3. **C)** Western blot and relative densitometry of
820 OVCAR5 whole cell lysates after treatment as in A in OVCAR5 cells. N=3. **D)** Percentage of ALDH+
821 cells using the ALDEFLUOR assay after treatment as in A in indicated cell lines. N=3. **E)** Images of
822 spheroids after pretreatment with mock (UT), cisplatin (3 h, ½ IC50), DAC (48 h, 100 nM) or DAC
823 (48 h, 100 nM) + cisplatin (3 h, ½ IC50). Scale bar = 500 μm. Graph depicts relative fluorescence
824 units (RFU) of CytoCalcein Violet 450 stain. N=4. For all panels, graphs indicate mean +/- SEM,
825 **P*<0.05, ***P*<0.001, ****P*<0.0001.

826

827 **Fig 5. G2/M cell cycle arrest results in an increase %ALDH+ cells. A)** Percentage of ALDH+ and
828 ALDH- cells in G1, S and G2/M phases of the cell cycle for indicated cell lines. N=3. **B)** Percentage
829 of ALDH+ and ALDH- cells in G1, S and G2/M phases of the cell cycle after mock (UT) or cisplatin
830 treatment (16 h, IC50) in OVCAR5 cells. **C)** Percentage of cells in G2/M after mock (UT), DMSO,
831 cisplatin (16 h, IC50) or CDK1 inhibitor (16 h, 9 μM) treatment in indicated cell lines. N=3. **D)** Total
832 percentage of ALDH+ cells treated as in C in indicated cell lines. N=3. For all panels, graphs
833 indicate mean +/- SEM, **P*<0.05, ***P*<0.001, ****P*<0.0001.

834

835 **Fig 6. NAMPT inhibition abrogates cisplatin-induced enrichment of ALDH+ cells. A)** Total NAD^+
836 (pmol/cells) in OVCAR5 cells after mock (UT) or cisplatin (16 h, IC50) treatment. N=3. **B)** Relative
837 *NAMPT* RNA expression after mock or cisplatin (IC50 dose) treatment for the indicated time
838 points and cell lines. N=3. **C)** Total NAD^+ (pmol/cells) in OVCAR5 cells after mock (UT), cisplatin
839 (16 h, IC50), NAMPTi (6 h, 50 nM), cisplatin (16 h, IC50) + DMSO or NAMPTi (6 h, 50 nM) + cisplatin
840 (16 h, IC50) treatment. N=3. **D)** Percentage of ALDH+ cells using the ALDEFLUOR assay after
841 treatment as in C in indicated cell lines. N=3. **E)** Images of spheroids after pretreatment with mock
842 (DMSO), cisplatin (3 h, ½ IC50), NAMPTi (6 h, 50 nM), or NAMPTi (6 h, 50 nM) + cisplatin treatment
843 (3 h, ½ IC50). Scale bar = 500 μm. Graph depicts relative fluorescence units (RFU) of CytoCalcein
844 Violet 450 stain. N=4. For all panels, graphs indicate mean +/- SEM, **P*<0.05, ***P*<0.001,
845 ****P*<0.0001.

846

847 **Fig 7. Cisplatin treatment induces two separate pathways to increase %ALDH+ cells. A)** Relative
848 *BRCA1* RNA expression after treatment with mock (UT), DMSO, cisplatin (16 h, IC50) or CDK1
849 inhibitor (16 h, 9 μM) treatment in indicated cell lines. N=3. **B)** Relative *NAMPT* RNA expression
850 after treatment as in A in indicated cell lines. N=3. **C)** Relative *NAMPT* RNA expression in
851 untransfected (UT) or transfected with mock empty vector (EV) or CpGi-null BRCA1 plasmid and
852 treated with or without cisplatin (16 h, IC50) in the indicated cell lines. For OVCAR5, * indicates
853 comparison between the indicated sample type and untransfected control with no treatment.
854 N=3. **D)** Total NAD^+ (pmol/cells) in untransfected (UT) or transfected with mock empty vector
855 (EV) or CpGi-null BRCA1 (BRCA1) plasmid and treated with or without cisplatin (16 h, IC50) in
856 OVCAR5 cells. N=3. **E)** Relative *NAMPT* RNA expression after mock (UT), cisplatin treatment (16
857 h, IC50), DAC (48 h, 100 nM) or DAC (48 h, 100 nM) + cisplatin (16 h, IC50) treatment in indicated
858 cell lines. N=3. For all panels, graphs indicate mean +/- SEM, **P*<0.05, ***P*<0.001, ****P*<0.0001,
859 *****P*<0.00001.
860
861 **Fig 8. Dual DNMTi and NAMPTi treatment abrogate cisplatin-induced OCSC enrichment. A)**
862 Percentage of ALDH+ cells using the ALDEFLUOR assay after treatment with mock (DMSO),
863 cisplatin (16 h, IC50), DAC (48 h, 10 nM or 20 nM) + cisplatin, NAMPTi (6 h, 12.5 nM) + cisplatin
864 treatment or NAMPTi +DAC + cisplatin treated in indicated cell lines. N=3. **B)** Combination index
865 plot for cells treated as described in A; x-axis represents fraction affected (Fa) and y-axis
866 represents combination index. Combinates beneath the dashed line are synergistic. **C)** Images of
867 spheroids after mock (DMSO), cisplatin (3 h, ½ IC50), DAC (48 h, 10 nM or 20 nM) + cisplatin,
868 NAMPTi (6 h, 12.5 nM) + cisplatin treatment or NAMPTi +DAC + cisplatin treated in indicated cell

869 lines. Scale bar = 500 μm. Graph depicts fluorescence intensity (RFU) of CytoCalcein Violet 450
870 stain. N=4. For all panels, Graphs depict mean +/- SEM. a indicates comparison between the
871 indicated sample type and DMSO treated sample. b indicates comparison between the indicated
872 sample type and cisplatin treated sample. c indicates comparison between the indicated sample
873 type and NAMPTi+ cisplatin treated sample. d indicates comparison between the indicated
874 sample type and DAC (10 nM) + cisplatin treated sample. e indicates comparison between the
875 indicated sample type and DAC (20 nM) + cisplatin treated sample. f indicates comparison
876 between the indicated sample type and NAMPTi + DAC (10 nM) + cisplatin treated sample.

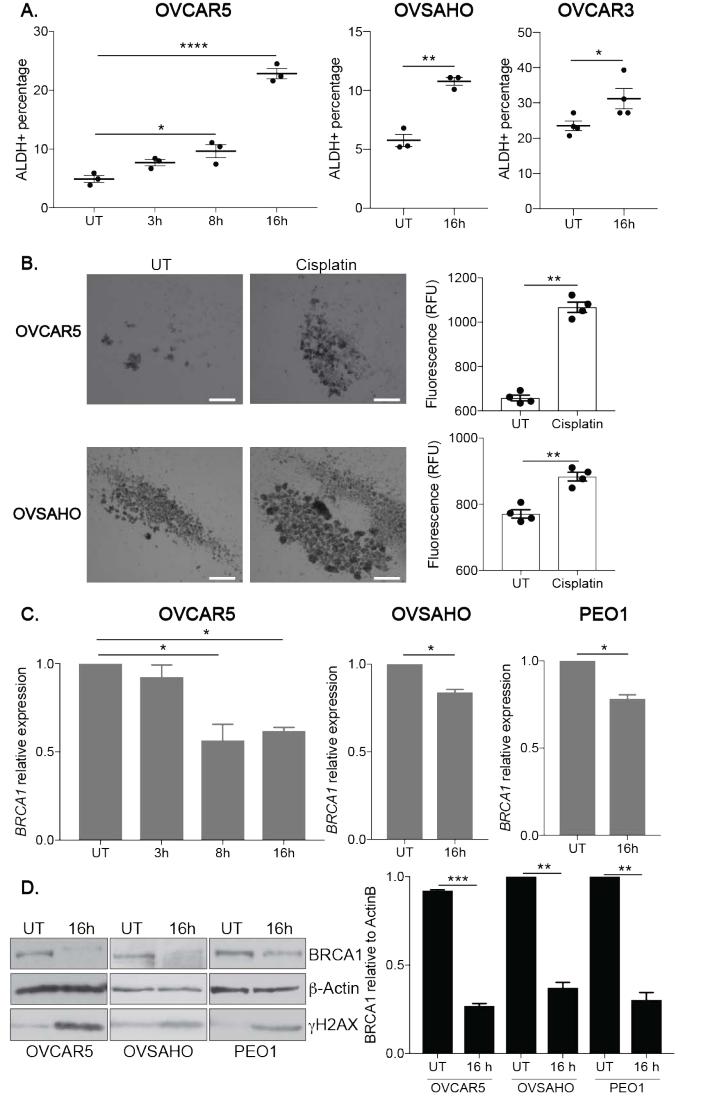
A.
OVCAR5
OVSAHO
OVCAR3
ALDH+ percentage
UT
3h
8h
16h
B.
UT
Cisplatin
OVCAR5
OVSAHO
Fluorescence (RFU)
C.
OVCAR5
OVSAHO
PEO1
BRCA1 relative expression
D.
BRCA1
β-Actin
γH2AX
BRCA1 relative to ActinB

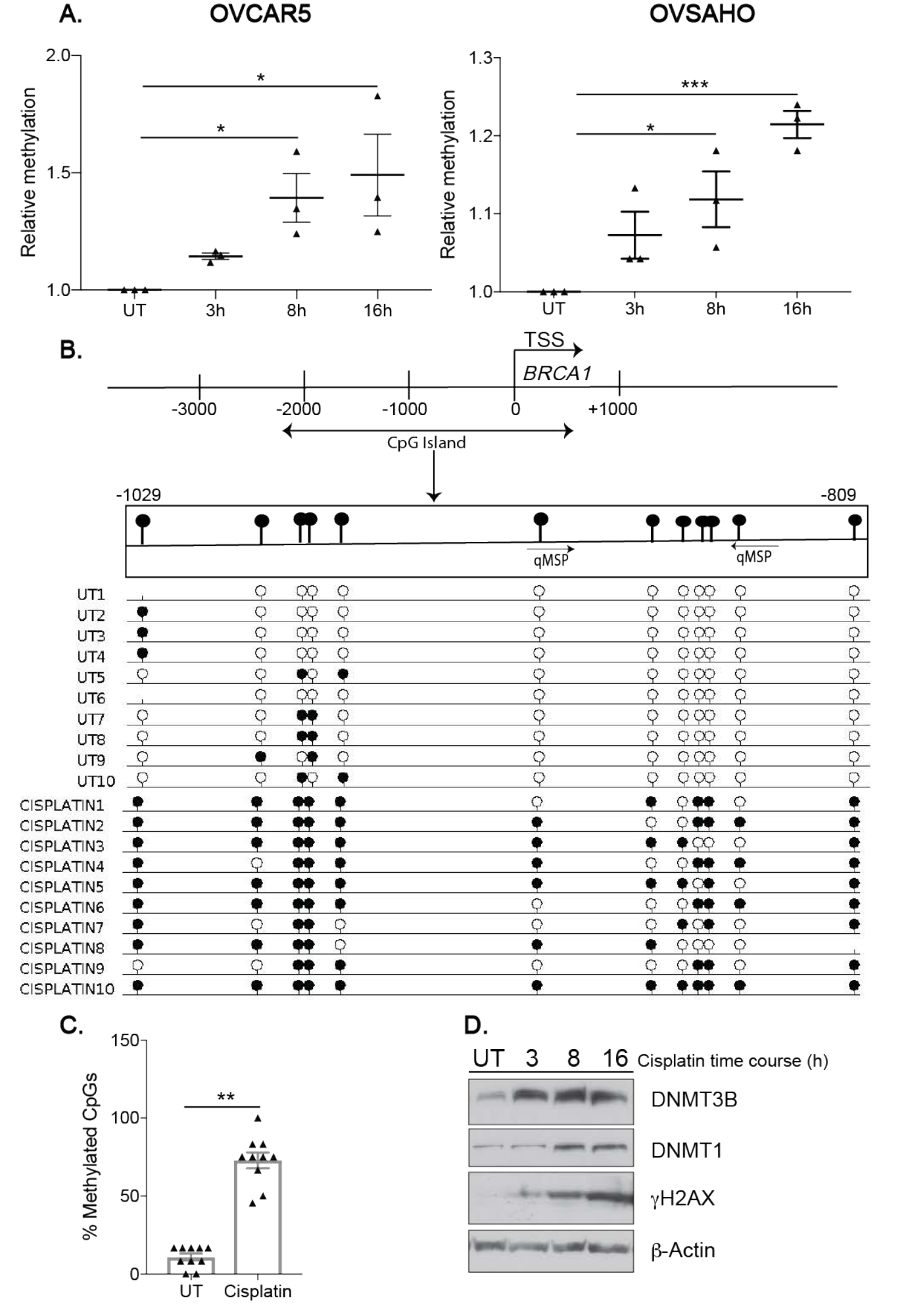
A.
OVCAR5
OVSAHO
Relative methylation
2.0
1.5
1.0
1.3
1.2
1.1
*
*
***
UT
3h
8h
16h
B.
TSS
BRCA1
-3000
-2000
-1000
0
+1000
CpG Island
-1029
-809
qMSP
qMSP
UT1
UT2
UT3
UT4
UT5
UT6
UT7
UT8
UT9
UT10
CISPLATIN1
CISPLATIN2
CISPLATIN3
CISPLATIN4
CISPLATIN5
CISPLATIN6
CISPLATIN7
CISPLATIN8
CISPLATIN9
CISPLATIN10
C.
% Methylated CpGs
150
100
50
0
**
UT
Cisplatin
D.
UT
3
8
16
Cisplatin time course (h)
DNMT3B
DNMT1
γH2AX
β-Actin

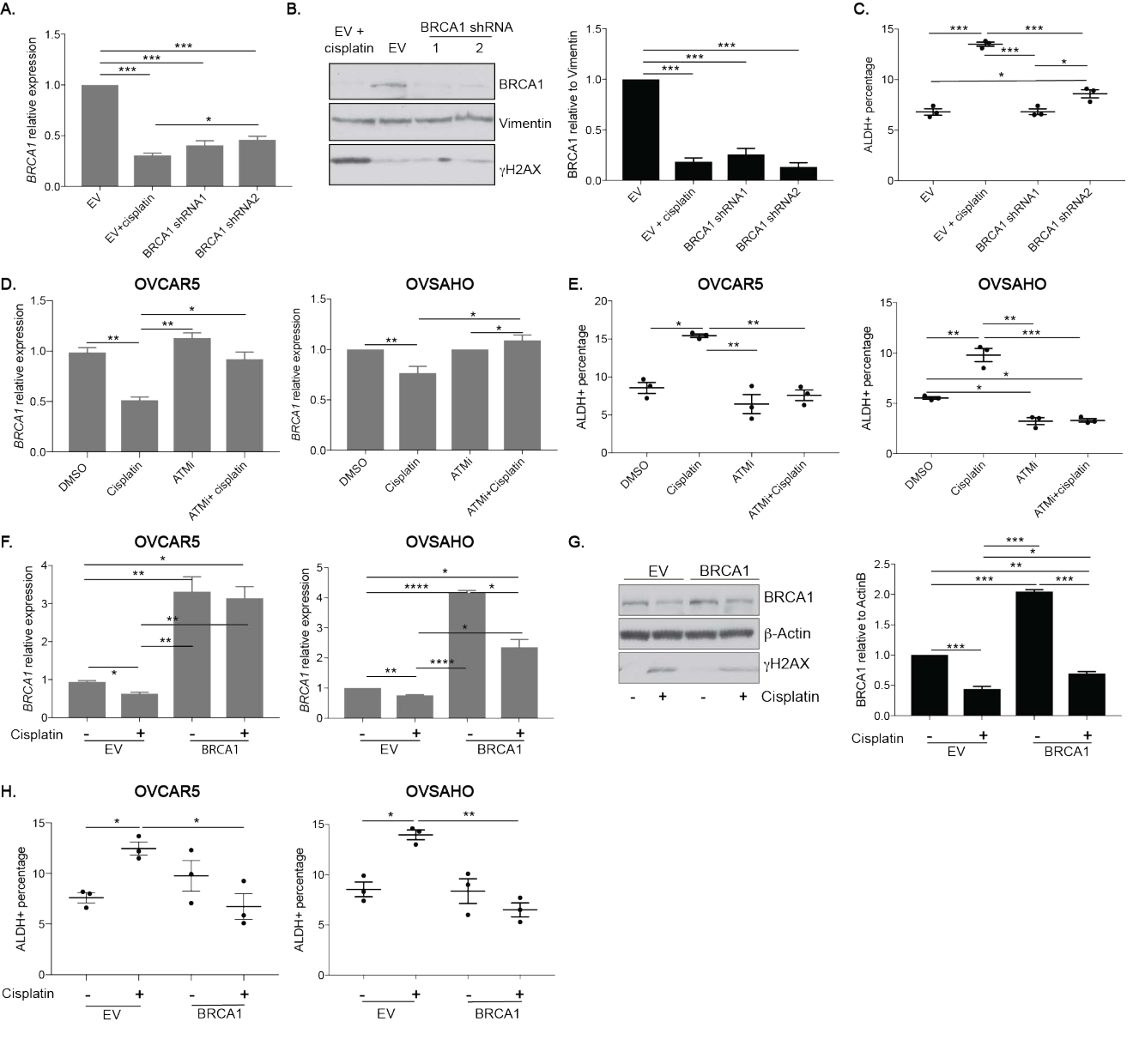
A.
BRCA1 relative expression
EV
EV+cisplatin
BRCA1 shRNA1
BRCA1 shRNA2
B.
EV + cisplatin
EV
BRCA1 shRNA
1
2
BRCA1
Vimentin
γH2AX
BRCA1 relative to Vimentin
C.
ALDH+ percentage
D.
OVCAR5
OVSAHO
DMSO
Cisplatin
ATMi
ATMi+ cisplatin
ATMi+Cisplatin
E.
F.
Cisplatin
G.
β-Actin
BRCA1 relative to ActinB
H.

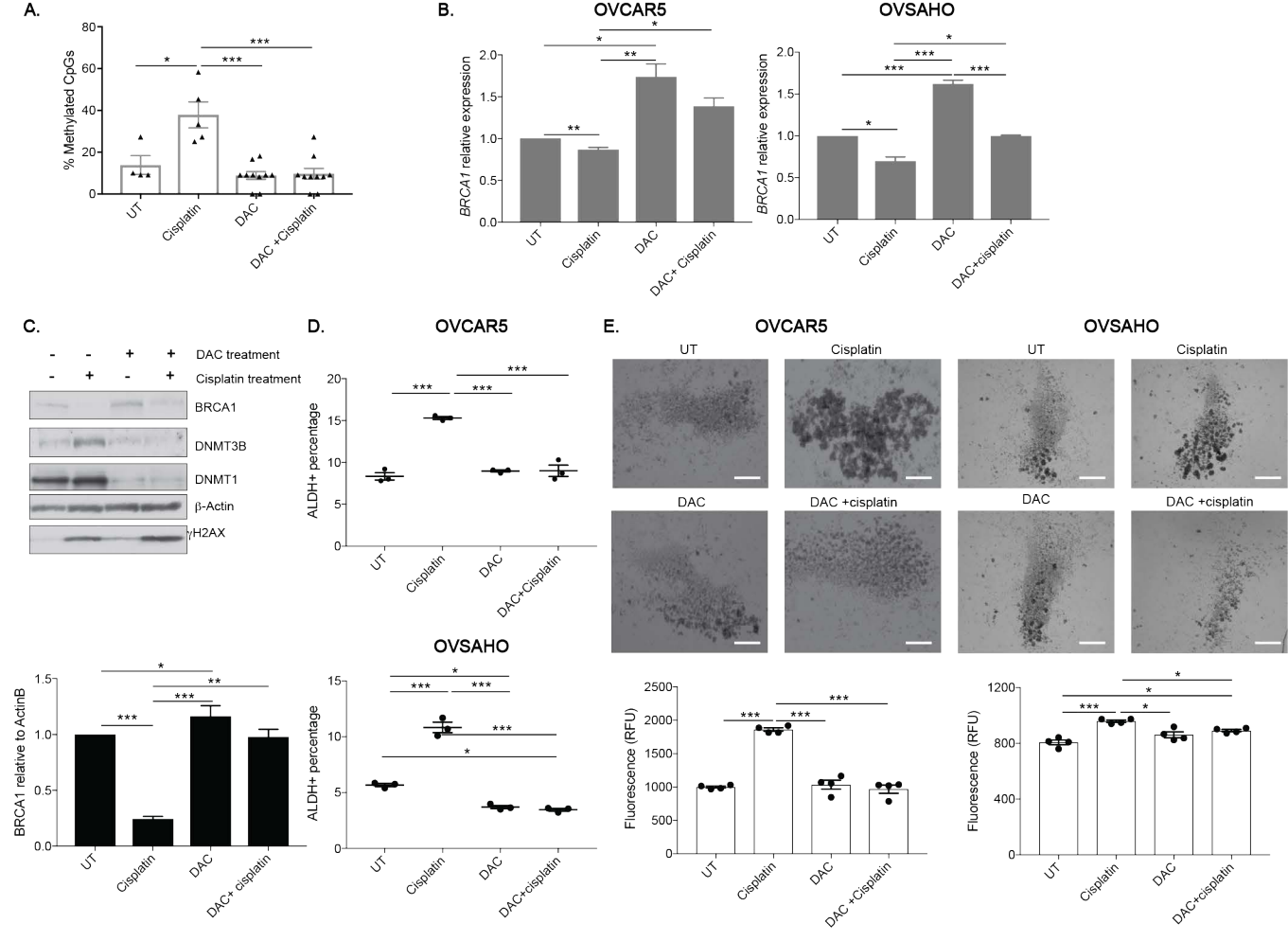
A.
% Methylated CpGs
UT
Cisplatin
DAC
DAC +Cisplatin
B.
OVCAR5
OVSAHO
BRCA1 relative expression
UT
Cisplatin
DAC
DAC+ Cisplatin
DAC+cisplatin
C.
DAC treatment
Cisplatin treatment
BRCA1
DNMT3B
DNMT1
β-Actin
γH2AX
BRCA1 relative to ActinB
D.
OVCAR5
OVSAHO
ALDH+ percentage
E.
OVCAR5
OVSAHO
UT
Cisplatin
DAC
DAC +cisplatin
Fluorescence (RFU)

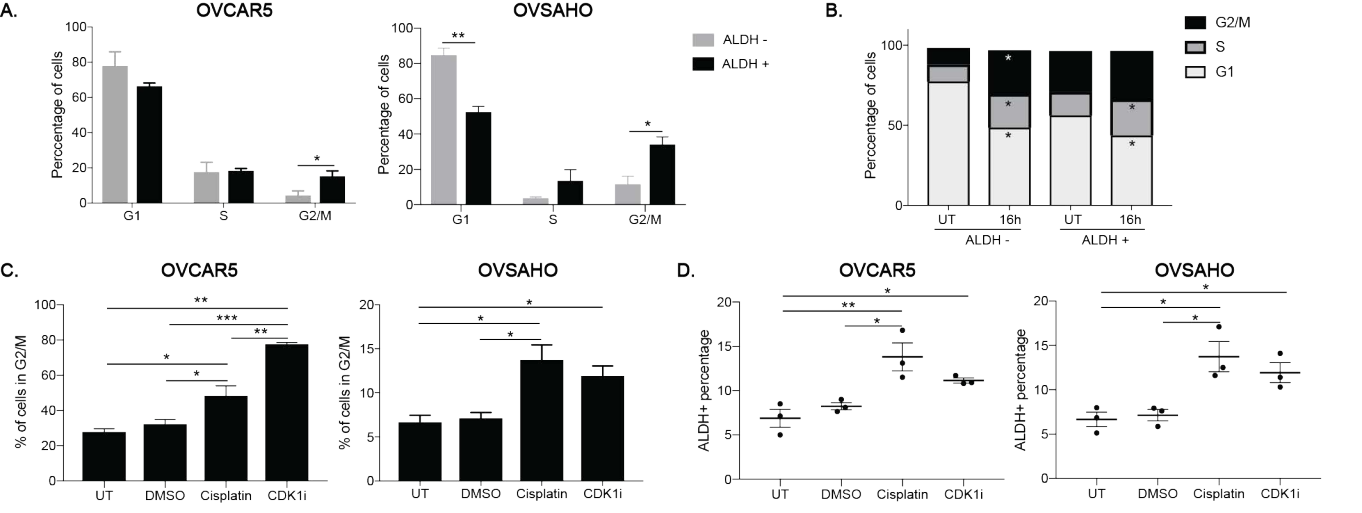
A.
OVCAR5
OVSAHO
Perccentage of cells
Percentage of cells
ALDH -
ALDH +
G1
S
G2/M
B.
G2/M
S
G1
UT
16h
ALDH -
ALDH +
C.
% of cells in G2/M
UT
DMSO
Cisplatin
CDK1i
D.
ALDH+ percentage

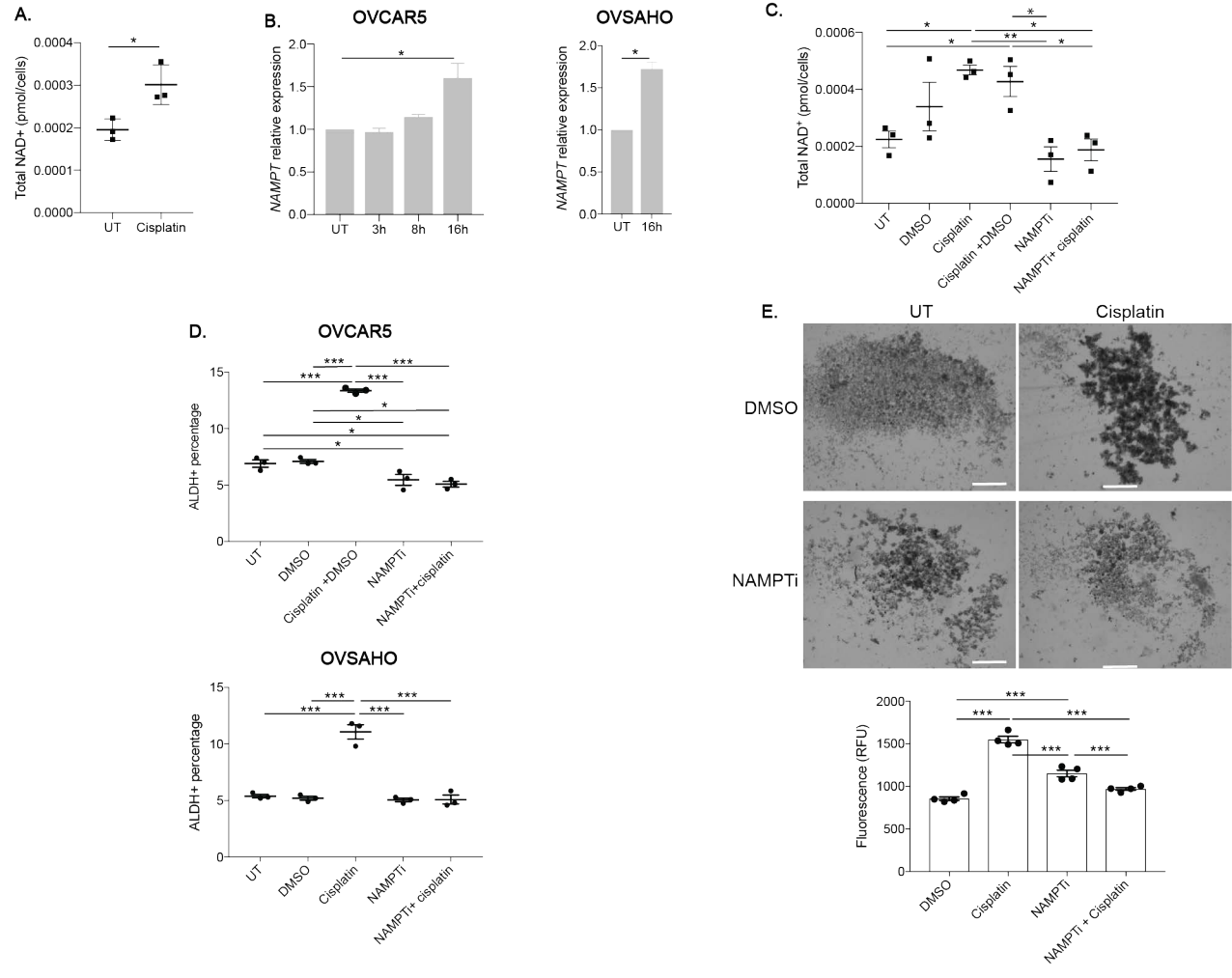
A.
Total NAD+ (pmol/cells)
0.0004
0.0003
0.0002
0.0001
0.0000
UT
Cisplatin
B.
OVCAR5
NAMPT relative expression
2.0
1.5
1.0
0.5
0.0
UT
3h
8h
16h
OVSAHO
NAMPT relative expression
UT
16h
C.
Total NAD+ (pmol/cells)
0.0006
0.0004
0.0002
0.0000
UT
DMSO
Cisplatin
Cisplatin +DMSO
NAMPTi
NAMPTi+ cisplatin
D.
OVCAR5
ALDH+ percentage
15
10
5
0
UT
DMSO
Cisplatin +DMSO
NAMPTi
NAMPTi+cisplatin
OVSAHO
ALDH+ percentage
UT
DMSO
Cisplatin
NAMPTi
NAMPTi+ cisplatin
E.
UT
Cisplatin
DMSO
NAMPTi
Fluorescence (RFU)
2000
1500
1000
500
0
DMSO
Cisplatin
NAMPTi
NAMPTi + Cisplatin

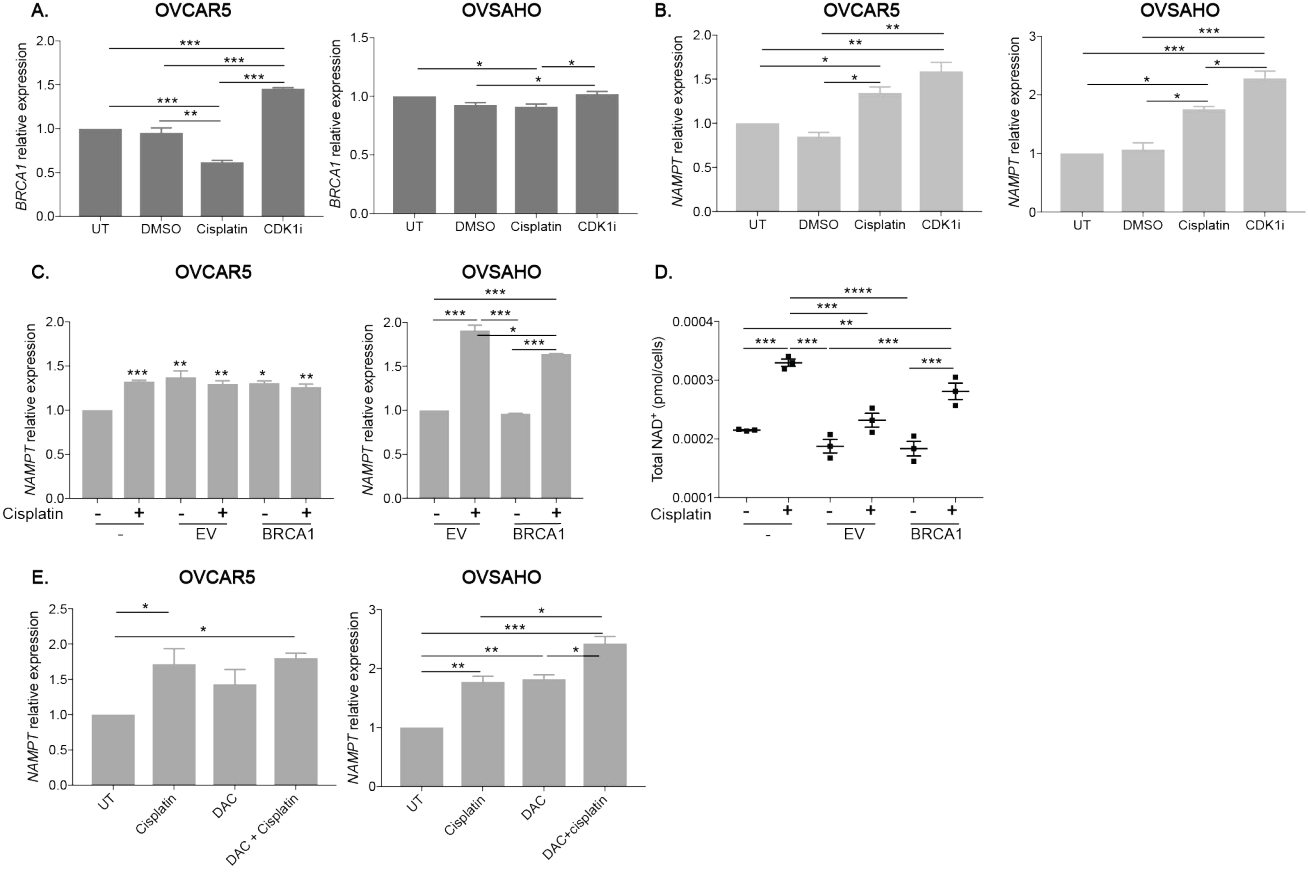
A.
OVCAR5
OVSAHO
BRCA1 relative expression
UT
DMSO
Cisplatin
CDK1i
B.
NAMPT relative expression
C.
Cisplatin
EV
BRCA1
D.
Total NAD+ (pmol/cells)
E.
DAC
DAC + Cisplatin
DAC+cisplatin

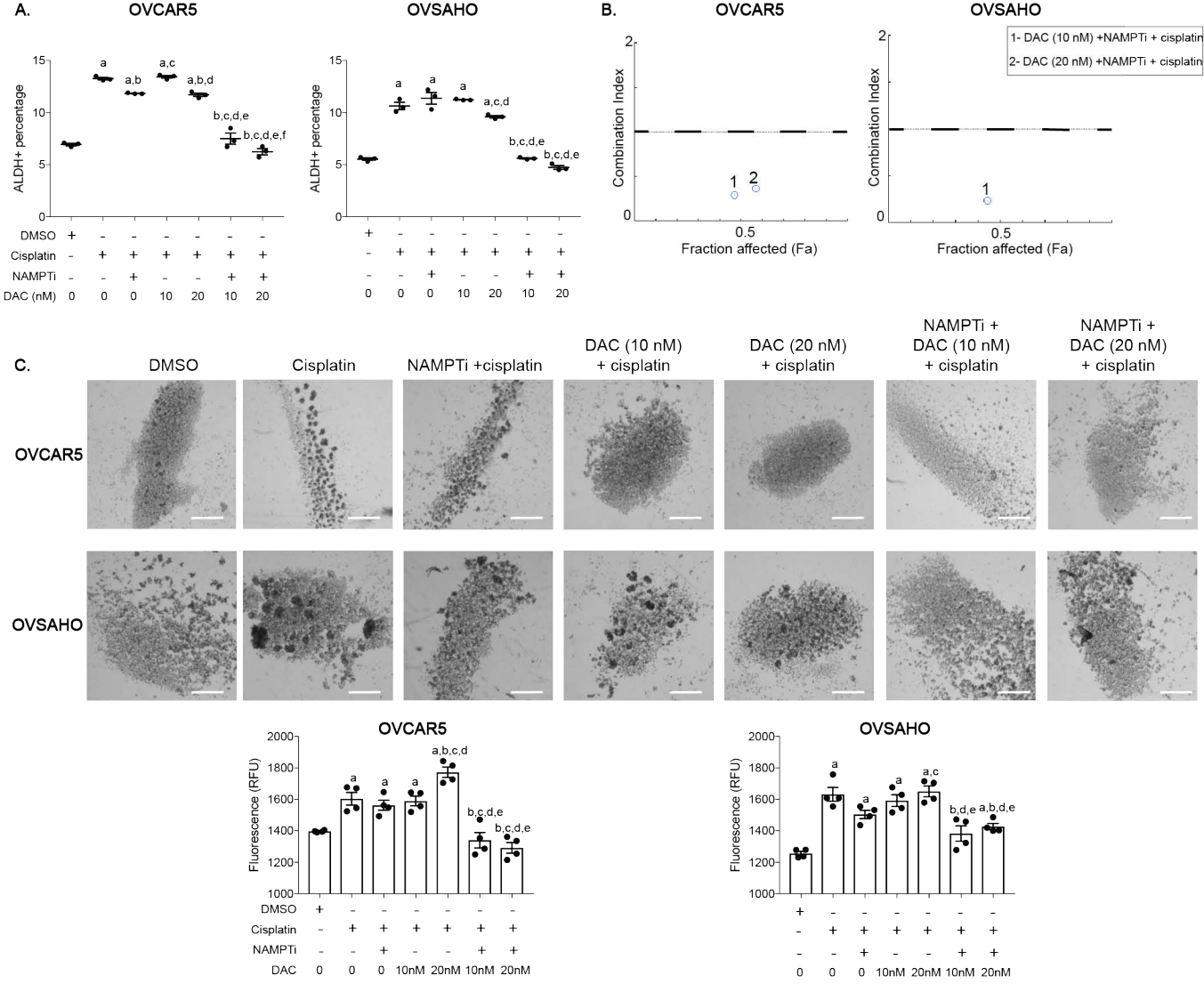
A.
OVCAR5
OVSAHO
ALDH+ percentage
DMSO
Cisplatin
NAMPTi
DAC (nM)
B.
OVCAR5
OVSAHO
1- DAC (10 nM) +NAMPTi + cisplatin
2- DAC (20 nM) +NAMPTi + cisplatin
Combination Index
Fraction affected (Fa)
C.
DMSO
Cisplatin
NAMPTi +cisplatin
DAC (10 nM) + cisplatin
DAC (20 nM) + cisplatin
NAMPTi + DAC (10 nM) + cisplatin
NAMPTi + DAC (20 nM) + cisplatin
OVCAR5
OVSAHO
Fluorescence (RFU)
DMSO
Cisplatin
NAMPTi
DAC
10nM
20nM